Research Square

Preprints are preliminary reports that have not undergone peer review.
They should not be considered conclusive, used to inform clinical practice,
or referenced by the media as validated information.

LRP1/AMPK/mTORC1 signaling in Large-Diameter Sensory Neurons Is Essential for TAFA4 Analgesia

Aziz Moqrich

aziz.moqrich@univ-amu.fr

CNRS UMR 7288

Aude Charron

Catarina Santos

Luc CAMOIN

INSERM U1068 https://orcid.org/0000-0002-1230-4787

Stephane AUDEBERT

Center of Research in Cancerology of Marseille (CRCM) https://orcid.org/0000-0002-9409-2588

Stéphane Gaillard

Francis Castets

Article

Keywords: TAFA4, LRP1, Aβ-LMTRs, AMPK, mTORC1, pain relief mechanism, novel therapeutic target

Posted Date: November 10th, 2026

DOI: https://doi.org/10.21203/rs.3.rs-11155467/v1

License: This work is licensed under a Creative Commons Attribution 4.0 International License.
Read Full License

Additional Declarations: Yes there is potential Competing Interest. AM is the co-founder and CSO of Tafalgie Therapeutics (TT). SG is cofounder and general manager of TT. AC and CS are research scientists of TT..

LRP1/AMPK/mTORC1 signaling in Large-Diameter Sensory Neurons Is Essential for TAFA4 Analgesia

Aude Charron[1,2], Catarina Santos[2], Luc Camoin[3], Stéphane Audebert[3], Stéphane Gaillard[2], Francis Castets[1,*] and Aziz Moqrich[1,2,4,*]

[1]Aix-Marseille-université, CNRS, Institut de Biologie du Développement de Marseille, UMR 7288, case 907, 13288 Marseille Cedex 09, France.

[2] Tafalgie Therapeutics, Parc Technologique Luminy 163 Avenue de Luminy Bâtiment CCIMP, 13009 Marseille

[3] Aix-Marseille Université, Inserm, CNRS, Institut Paoli-Calmettes, CRCM, Marseille Protéomique, Marseille, France.

[4] Lead contact

*Corresponding author: aziz.moqrich@univ-amu.fr ; francis.castets@univ-amu.fr

ABSTRACT

Pain, whether acute or persistent, represents a major global medical challenge. Despite decades of research, current analgesic strategies remain largely unsatisfactory, in part because most therapies repeatedly target the same receptors or ion channels involved in inflammation or central nervous system activity. Here, we identify a distinct peripheral pathway that directly modulates a defined subset of sensory neurons to relieve pain. We show that the secreted protein TAFA4 exerts analgesic effects by signaling through the Low-Density Lipoprotein Receptor-Related Protein 1 (LRP1) in large-diameter sensory neurons. This signaling activates AMPK, which in turn inhibits mTORC1, a key driver of neuronal sensitization. Pharmacological blockade of AMPK or forced activation of mTORC1 abolishes TAFA4-induced analgesia, confirming the central role of the LRP1/AMPK/mTORC1 axis. Our findings reveal a previously unrecognized sensory neuron pathway that mediates pain relief and highlight a promising molecular target for the development of peripheral analgesics.

Key words: TAFA4, LRP1, Aβ-LMTRs, AMPK, mTORC1, pain relief mechanism, novel therapeutic target

INTRODUCTION

Chronic pain affects more than 30% of the global population and remains difficult to treat because current analgesics primarily target a limited set of central or inflammatory pathways, often with modest efficacy and significant side effects [1]. Targeting the peripheral nervous system (PNS) offers a promising alternative by reducing pain while minimizing the adverse effects associated with centrally acting therapies. Within the PNS, sensory neurons of the dorsal root ganglia (DRG) play a pivotal role in relaying somatosensory information from the skin, muscles, and viscera to the CNS. These neurons encompass diverse subtypes, including low-threshold mechanoreceptors (LTMRs) that detect innocuous tactile stimuli, and nociceptors, which respond selectively to noxious signals [2, 3, 4].

Among LTMRs, Aβ-LTMRs are large-diameter, heavily myelinated neurons specialized in discriminative touch and vibration sensation [5]. Classic and contemporary studies have demonstrated that activation of Aβ-LTMRs can inhibit nociceptive transmission under physiological conditions [6, 7, 8]. However, their role in modulating injury-induced pain remains controversial. While some studies have shown that ablation or local activation of Aβ-RA-LTMRs enhances mechanical nociception after injury [9, 10, 11], others demonstrated that their global activation at the spinal level alleviates inflammatory and neuropathic mechanical pain [9]. Together, these findings suggest that pain modulation involves a delicate balance between Aβ-LTMR excitation and inhibition, raising the possibility that selective molecular control of these neurons could offer a powerful strategy for treating mechanical allodynia.

Our laboratory previously identified TAFA4, a secreted protein enriched in C-LTMRs projecting to lamina IIi of the dorsal horn, as a potent modulator of injury-induced pain [12, 13, 14, 15, 16]. TAFA4 deficiency increases dorsal horn excitability and prolongs inflammatory and neuropathic pain, whereas recombinant TAFA4 reverses these effects [12, 14, 16, 17].

Mechanistically, TAFA4 enhances inhibitory synaptic transmission and restores neuronal ionic conductances through the low-density lipoprotein receptor-related protein 1 (LRP1) [16]

LRP1 is a multifunctional receptor involved in endocytosis, cellular signaling, and lipid metabolism [18]. Its role in modulating inflammation and tissue repair has implicated it in diverse pathologies, including cancer, atherosclerosis, and organ injury [19, 20]. Within the nervous system, LRP1 regulates Schwann cell function, microglial activation, and neuronal excitability; processes intimately linked to pain pathogenesis [21, 22, 23, 24]. Notably, LRP1 deletion in Schwann cells leads to spontaneous mechanical allodynia, whereas its loss in microglia reduces neuropathic pain after nerve injury [25, 26, 27, 28]. Despite these insights, the contribution of neuronal LRP1 to pain modulation has remained unexplored.

Here, we demonstrate that LRP1 in sensory neurons, particularly in large-diameter Aβ-LTMRs, is essential for TAFA4-induced analgesia across inflammatory, postoperative, and neuropathic pain models. Through genetic, biochemical, and phosphoproteomic approaches, we reveal that TAFA4 binding to neuronal LRP1 activates AMP-activated protein kinase (AMPK), which subsequently inhibits mTORC1, a central driver of neuronal sensitization. Pharmacological blockade of AMPK or forced activation of mTORC1 abolishes TAFA4-mediated analgesia, establishing the LRP1/AMPK/mTORC1 axis as a key regulatory pathway for peripheral pain relief. These findings uncover a previously unrecognized molecular mechanism through which a secreted protein modulates large-diameter sensory neurons to alleviate pain, identifying a promising peripheral target for next-generation analgesics.

RESULTS

Sensory Neurons' LRP1 is Required for the Analgesic Effect of TAFA4

In a recent study, we showed that intrathecal (IT) and subcutaneous (SC) administration of human recombinant TAFA4 reversed inflammatory, postoperative and nerve injury-induced mechanical hypersensitivity, demonstrating that TAFA4 acts at both spinal and peripheral levels [16]. To further dissect the spinal versus peripheral roles of TAFA4, we performed a series of dual injections of TAFA4 and the LRP1 inhibitor RAP (receptor-associated protein). As previously shown, IT injection of RAP completely abolished TAFA4 analgesic effect when TAFA4 was administered intrathecally (**Fig. 1A**). Similarly, SC co-administration of RAP and TAFA4 also abolished the analgesic effect of TAFA4 (**Fig. 1B**). In contrast, the analgesic effect of SC injection of TAFA4 was not affected by IT injection of RAP (**Fig. 1C**) suggesting that TAFA4 also exerts its analgesic effect at the peripheral level and does not necessarily require passage across the blood–brain barrier. LRP1 is highly expressed in satellite and Schwann cells [29]. However, its expression in DRG neurons is poorly documented. To address the role of peripheral LRP1 in the analgesic effect of TAFA4, we took advantage of LRP1 conditional knockout mice [30]. We first crossed these mice with mice that express the tamoxifen-inducible CRE recombinase from the proteolipid protein 1 promoter (*plp1*$^{CRE\text{-}ert2}$) (hereafter called *Plp1-LRP1*) (**Fig. 1D** and *SI Appendix Fig. S1A*). As expected, LRP1 protein was efficiently depleted in satellite glial cells (*SI Appendix Fig. S1B*) and Schwann cells (*SI Appendix Fig. S1D–E*). Loss of LRP1 in Schwann cells led to structural abnormalities, including defects in axon myelination and impaired ensheathment of axons by non-myelinating Schwann cells within Remak bundles (*SI Appendix Fig. S1C*). Next, we sought to evaluate the analgesic effect of TAFA4 in *Plp1-LRP1* mice. We used the Spared Nerve Injury (SNI) as a model of neuropathic pain. Consistent with Orita and colleagues [29], *Plp1-LRP1* mice exhibited pronounced mechanical allodynia at baseline levels. Seven days post-SNI both *lrp1*$^{flx/flx}$ (hereafter named control) and *Plp1-LRP1* mice developed robust SNI-induced mechanical hypersensitivity (**Fig. 1E and F**). Notably, both SC and IT administration of TAFA4 reversed SNI-induced

mechanical hypersensitivity in both genotypes (**Fig. 1E and F**), demonstrating that LRP1 in satellite and Schwann cells is not required for the analgesic effect of TAFA4.

Next, we selectively depleted LRP1 in primary sensory neurons by crossing*lrp1*$^{flx/flx}$ mice with transgenic mice expressing the CRE recombinase under the control of the Advillin promoter *Advillin*$^{CRETg/+}$ hereafter referred to as *Advillin-LRP1* mice [31] (**Fig. 1G** and *SI Appendix S1F*). As the *lrp1* gene is highly expressed in satellite cells, we were unable to confirm the loss of LRP1 protein in DRG neurons by immunohistochemistry (*SI Appendix Fig. S1G*). As an alternative, we performed RNAscope analysis and found that *Lrp1* transcripts were markedly reduced in DRG neurons (*SI Appendix Fig. S1L and M*). DRG neurons from *Plp1-LRP1* mice were used as controls to show that in this mouse model *lrp1* gene was not affected in DRG neruons (*SI Appendix Fig. S1N).*

To determine whether the loss of LRP1 in sensory neurons affected TAFA4-mediated analgesia, we used the Spared Nerve Injury (SNI) model of neuropathic pain. Deletion of LRP1 had no effect on baseline mechanical thresholds. Seven days after SNI, both control and *Advillin-LRP1* mice developed strong mechanical hypersensitivity. Subcutaneous (SC) injection of TAFA4 reversed SNI-induced hypersensitivity in control mice but not in *Advillin-LRP1* mice (**Fig. 1H**). In contrast, intrathecal (IT) administration of TAFA4 reversed SNI-induced hypersensitivity in both genotypes (**Fig. 1I**). In the same pain model, SC injection of pregabalin or IT injection of baclofen, SNC80, or DAMGO effectively reduced mechanical hypersensitivity in both genotypes (*SI Appendix Fig. S1H–K*), confirming the preserved responsiveness to other analgesic agents in *Advillin-LRP1* mice. We further extended this analysis to three additional pain models: postoperative pain (paw incision), inflammatory pain (intraplantar carrageenan injection), and neuropathic pain induced by chronic constriction injury (CCI) of the sciatic nerve. In all models, SC injection of TAFA4 failed to produce analgesia in *Advillin-LRP1* mice (**Fig. 1J–L**). These findings demonstrate that LRP1 in primary

sensory neurons, but not in satellite or Schwann cells, is essential for the analgesic effect of TAFA4.

To confirm the findings obtained with *Advillin-LRP1* mice and to begin identifying the specific LRP1-expressing neuronal populations mediating TAFA4's analgesic effect, we next used, the Nav1.8^{CRE} mice (hereafter referred to as *Nav1.8-LRP1*) (**Fig. 2A**). This mouse line targets LRP1 deletion in nearly all small-diameter sensory neurons, including Aδ-nociceptors, but not in TrkB-expressing Aδ-LTMRs or in a subset of Aβ-LTMRs [32]. *Nav1.8-LRP1* mice were subjected to the paw incision model, and the analgesic effect of TAFA4 was evaluated one day post-injury. While subcutaneous (SC) injection of TAFA4 produced a robust analgesic effect in control mice, this effect was completely absent in *Nav1.8-LRP1* mice (**Fig. 2B**). In contrast, intrathecal (IT) administration of TAFA4 effectively reversed paw incision-induced mechanical hypersensitivity in both genotypes (**Fig. 2C**), indicating that LRP1 in neurons of the Nav1.8 lineage is essential for the peripheral analgesic effect of TAFA4.

To further refine the identity of LRP1-expressing neurons involved in TAFA4-mediated analgesia, we used two additional mouse models targeting distinct subsets within the Nav1.8 lineage: the *GINIP-DTR* mice [13] and the resiniferatoxin (RTX)-treated mice. The *GINIP-DTR* model allows selective ablation of mechano-nociceptive MRGPRD-expressing neurons and C-LTMRs, while RTX treatment ablates TRPV1-expressing C- and Aδ-nociceptors. Both models were subjected to paw incision, and mechanical hypersensitivity was assessed one day after injury. In both cases, SC administration of TAFA4 produced significant analgesia irrespective of genotype or neuronal ablation (**Fig. 2D-I**), demonstrating that neither C-fibers nor Aδ-nociceptors are required for TAFA4's analgesic action.

Molecular and functional validations of the *GINIP-DTR* and RTX models are shown in Figures S2A and S2B. Specifically, *GINIP-DTR* mice exhibited a marked reduction in IB4 and TH immunostaining (*SI Appendix Fig. S2A*), confirming the efficient ablation of MRGPRD-

positive and C-LTMR neurons, whereas RTX-treated mice displayed increased response latency to noxious thermal stimuli in the tail flick test (*SI Appendix Fig. S2B*).

The Analgesic Effect of TAFA4 Is Mediated Through LRP1 in a Subset of Aβ-LTMRs

Since the analgesic effect of TAFA4 was abolished in *Advillin-LRP1* and *Nav1.8-LRP1* mice, and considering that C-fibers, Aδ-nociceptors, and Aδ-LTMRs were shown to be dispensable based on results from the *Nav1.8-LRP1*, *GINIP-DTR*, and RTX models, we hypothesized that TAFA4 exerts its analgesic effect through a subset of LRP1-expressing Aβ-LTMRs targeted by both the $Nav1.8^{CRE}$ *and the* $Advillin^{CRE}$ lines. To identify these neurons, we crossed the two mouse lines with CRE-dependent Ai14 ($Rosa26^{flx\text{-}Stop\text{-}flx\text{-}tdTomato}$) reporter mice to generate *Nav1.8-tdTomato* and *Advillin-tdTomato* mice. In both reporter lines, we performed double immunostaining on lumbar DRG sections and quantified the proportion of $NF200^+$ and $CGRP^+$ neurons co-expressing tdTomato. As expected, approximately 50% of $NF200^+$ neurons co-expressed tdTomato in *Nav1.8-tdTomato* mice, and 85% of $NF200^+$ neurons did so in *Advillin-tdTomato* mice (**Fig. 3A**). Interestingly, while 95% of $CGRP^+$ neurons co-expressed tdTomato in *Nav1.8-tdTomato* mice, only 50% of these neurons did so in *Advillin-tdTomato* mice (**Fig. 3B**). In line with this, triple labeling confirmed that a large proportion of $CGRP^+/NF200^+$ lack the expression of td-Tomato, further confirming the absence of CRE-recombination in these neurons in *Advillin-tdTomato* mice (*SI Appendix Fig. S2C*). Although this was unexpected, since Advillin is reported to be expressed in all DRG neurons, this finding aligns with the preserved TAFA4 analgesic effect observed in RTX-treated mice (**Figs. 2G**, **2H**) and further supports the hypothesis that TAFA4 acts through a subset of Aβ-LTMRs targeted by both $Advillin^{CRETg}$ and the $Nav1.8^{CRE}$ lines.

To further characterize this subset, we performed double immunostaining with anti-RFP in combination with either TrkC or parvalbumin (PV), two established molecular markers of Aβ-LTMRs. In *Advillin-tdTomato* mice, 89% of $TrkC^+$ neurons and 92% of PV^+ neurons expressed

tdTomato, whereas only 39% of TrkC^{+} neurons and 11% of PV^{+} neurons did so in *Nav1.8-tdTomato* mice (**Figs. 3C, 3D**). By contrast, similar proportions of P2X3^{+} and tyrosine hydroxylase (TH)$^{+}$ neurons expressed tdTomato in both reporter lines (**Fig. 3E, 3F, 3G)**, indicating that these non-Aβ-LTMR populations are targeted comparably by the Advillin^{Cre} and Nav1.8^{Cre} drivers. Publicly available single-cell RNA sequencing data classify NF200^{+} neurons into five distinct subsets (NF1 to NF5) [33]. Based on these datasets, NF1 and NF3 populations can be excluded as they do not express *Lrp1*. Our expression analyses indicate that a subset of TrkC^{+} and PV^{+} neurons, targeted by both *Advillin^{CRE}* and the *Nav1.8^{CRE}* mouse lines, co-express LRP1 within the NF2, NF4, and NF5 populations. We therefore conclude that the Aβ-LTMRs belonging to the NF2, NF4, and NF5 subsets are the most likely neuronal subpopulations mediating TAFA4's analgesic effects (*SI Appendix Fig. S2D*).

TAFA4/LRP1 Increases Phosphatase Activity in Large Diameter DRG Neurons

To provide mechanistic insights into how TAFA4 mediates its analgesic action, we reasoned that a comprehensive assessment of the protein complexes proximal to its receptor LRP1 might be valuable. HA-tagged TAFA4 was attached to anti-HA beads and the complex was used to pull-down brain plasma membrane proteins. The control experiment consisted of pulling down plasma membrane proteins in the absence of HA-TAFA4. Controls and HA-TAFA4 complexes were subjected to LC-MS/MS. Protein identification and quantification was processed using the MaxQuant [34] and Perseus softwares [35]. 1799 proteins were identified and 280 were enriched in HA-TAFA4 in comparison to the control condition at 1% FDR (**Fig. 4A**). Gene ontology (GO) and String (https://string-db.org/) pathway analyses revealed a significant enrichment in protein phosphatase type 2A complex (**Fig. 4B**).

PP2A is an essential and versatile Serine/Threonine phosphatase that regulates the activity of more than 30 different kinases, including protein kinase B (AKT), PKC, p70 S6 kinase, cAMP dependent kinases, CAM-kinase and ERK/MAP kinase [36]. To test whether TAFA4 modulates

general phosphatase activity, overnight DRG cultures were treated with TAFA4 or vehicle for 45 minutes at 37°C. Cell homogenates were incubated with DiFMUP (6,8-Difluoro-4-Methylumbelliferyl Phosphate) and the fluorescence intensity of hydrolyzed DiFMU was monitored every 3 minutes for 30 minutes (**Fig. 4C, 4D**). For all experiments, data were normalized to the phosphatase activities of vehicle-treated cultures. Under these conditions, phosphatase activity was significantly increased in DRG neurons treated with TAFA4 compared to vehicle treatment (**Fig. 4E**). To test whether the TAFA4-mediated increase in phosphatase activity was LRP1 dependent, we performed the same experiments using DRG cultures from *Advillin-LRP1*, *Nav1.8-LRP1, PLP1-LRP1, GINIP-DTR* and RTX mice. TAFA4 induced a significant increase in phosphatase activity in DRGs from all control mice compared to vehicle treatment. However, TAFA4 effect was significantly impaired in cultured DRGs from *Advillin-LRP1* and *Nav1.8-LRP1* mice (**Fig. 4F**). Consistent with our behavioral data, the TAFA4-mediated increase in phosphatase activity was not affected in *Plp1-LRP1*, *GINIP-DTR* and RTX mice (**Fig. 4G**). Taken together, our data demonstrate that TAFA4/LRP1 signaling acts as a potent modulator of phosphatase activity mainly in Aβ-LTMRs.

TAFA4-mediated pain relief effect occurs through negative modulation of mTORC1 signaling

Since we have demonstrated that TAFA4 positively modulates phosphatase activity, we hypothesized that it does so by modulating protein phosphorylation. To test this, we treated DRG cultures with either vehicle or TAFA4 and processed the cell lysates for TMT-16plex isobaric labeling [37]. Phosphopeptide enrichment was carried out using MagReSyn beads (ReSyn Biosciences), followed by mass spectrometry analysis on an Orbitrap Fusion Lumos Tribrid Mass Spectrometer. Differentially phosphorylated peptides were identified and quantified using MaxQuant [34], revealing 1,017 phosphorylation sites, of which 824 were class 1 phosphopeptides with precise localization. Among these, 13 sites from 8 proteins were found

to be differentially phosphorylated (5% FDR), with 11 sites up-regulated (Add2, Esyt1, Wdr1, Azin2, Kcnn3, Garin2, Irf2bp2) and 2 down-regulated on Npat. Using PhosphoSite (www.phosphosite.org), we found that 5 of the 8 identified proteins have been functionally linked to mTORC1 signaling.

To validate the involvement of TAFA4 in modulating mTORC1 signaling, we treated DRG cultures from control and *Advillin-LRP1* mice with either vehicle or TAFA4, followed by immunocytochemistry and Western blot analysis. TAFA4 significantly decreased mTORC1 phosphorylation in control, but not in *Advillin-LRP1* DRG cultures, without altering total mTORC1 protein levels (**Fig. 5A**). Quantitative analysis of immunostaining intensity further confirmed the TAFA4-induced reduction in mTORC1 phosphorylation, which was abolished in Advillin-LRP1 DRG cultures (**Figs. 5E**). These findings support a critical role for LRP1 in mediating the TAFA4-dependent negative regulation of mTORC1 activity in Aβ-LTMRs.

To further substantiate the inhibitory effect of TAFA4 on mTORC1 signaling, we assessed the phosphorylation status of its downstream effector, p70 S6 kinase (p70 S6K). Consistent with the findings above, treatment of DRG cultures with TAFA4 significantly reduced p70 S6K phosphorylation (**Fig. 5F**), further supporting the inhibitory effect of TAFA4 on the mTORC1 signaling pathway.

Next, we sought to identify the upstream signaling pathway through which TAFA4/LRP1 interaction induces mTORC1 dephosphorylation. The PI3K/AKT and AMPK pathways are well established as positive and negative regulators of mTORC1 activity, respectively [38, 39]. To determine which pathway was engaged, we treated DRG cultures with TAFA4 or vehicle and performed Western blot analyses. TAFA4 treatment led to a marked increase in AMPK phosphorylation, accompanied by a modest reduction in ERK and AKT phosphorylation levels (**Fig. 5G and H**).

To evaluate whether these in vitro findings translate *in vivo*, we used compound C, an AMPK inhibitor, to test whether blocking AMPK activity would prevent TAFA4-mediated analgesia. Using the paw incision model, we compared the effects of compound C alone, TAFA4 alone, and their co-administration. As expected, subcutaneous (SC) administration of TAFA4 alone produced a strong analgesic effect at one- and two-hours post-administration (**Fig. 5I**). Intraplantar (IP) injection of compound C alone had no effect on mechanical hypersensitivity; however, IP pretreatment with compound C markedly reduced the analgesic effect of TAFA4 (**Fig. 5I**).

To further support these findings, we genetically perturbed mTORC1 signaling. Specifically, we inactivated *Tsc2*, a negative regulator of mTORC1, in sensory neurons by generating mice with a conditional deletion of *Tsc2* in the Advillin lineage (hereafter referred to as *Advillin-TSC2* mice). To test whether enhanced mTORC1 activation interferes with TAFA4-induced analgesia, *Advillin-TSC2* and control ($Tsc2^{flx/flx}$) littermates were subjected to the paw incision model. Both genotypes developed robust incision-induced mechanical hypersensitivity. However, SC administration of TAFA4 produced significant analgesia in control mice, but not in *Advillin-TSC2* mice (**Fig. 5J**). Taken together, our in vitro and in vivo data demonstrate that TAFA4-mediated analgesia depends on the negative modulation of mTORC1 activity in Aβ-LTMRs through the TAFA4/LRP1/AMPK/mTORC1 signaling axis.

DISCUSSION

In this study, we identify a previously unrecognized molecular mechanism through which the neuropeptide TAFA4 mediates analgesia via LRP1 signaling in a subset of Aβ-LTMRs. By combining genetic, pharmacological, and proteomic approaches, we demonstrate that TAFA4/LRP1 signaling promotes a phosphatase-dependent downregulation of mTORC1 activity through the activation of the AMPK pathway. This cascade ultimately results in a reduction of neuronal excitability and pain hypersensitivity. Together, our findings reveal a

novel LRP1-dependent modulatory axis within peripheral sensory neurons that contributes to the control of pain signaling.

Using cell type–specific conditional knockout strategies, we show that LRP1 in sensory neurons, but not in Schwann or satellite glial cells, is essential for TAFA4-mediated analgesia. This distinction is critical, as previous studies have implicated glial LRP1 primarily in myelination and nerve repair processes [27, 29], whereas our data establish a direct neuronal role for LRP1 in pain modulation. The observation that intrathecal administration of TAFA4 retained efficacy in *Advillin-LRP1* mice further supports the notion that distinct LRP1 pools in spinal and peripheral compartments contribute separately to the dual site of TAFA4 action.

Through conditional deletion and neuronal ablation studies, we excluded C-fibers, Aδ-nociceptors, and Aδ-LTMRs as primary mediators of TAFA4's peripheral action. Instead, LRP1-expressing Aβ-LTMRs emerge as the critical population. This aligns with evidence that subsets of Aβ afferents can exert antinociceptive functions under pathological conditions. Specifically, the overlap of Advillin^{CRE} and Nav1.8^{CRE} recombination patterns within NF2, NF4, and NF5 neuronal subsets, co-expressing LRP1, TrkC, and parvalbumin, identifies the most likely TAFA4-responsive population. The role of Aβ-LTMRs in initiating or maintaining injury-induced central sensitization and touch-evoked pain has long been recognized. Ectopic activity in Aβ fibers has been implicated in various neuropathic conditions [40, 41, 42, 43, 44]. Blocking Aβ-LTMR activity in humans or mice attenuates mechanical hypersensitivity [45], while optogenetic activation of SplitCre-Aβ-LTMRs evokes mechanical nociception under chronic inflammatory and neuropathic pain conditions [9]. In contrast, genetic or pharmacological ablation of C-fibers did not prevent the onset of injury-induced central sensitization and mechanical hypersensitivity [13, 41, 46, 47, 48, 49], highlighting the critical contribution of Aβ-LTMRs in how touch is pathologically converted into pain.

What are the molecular mechanisms that underlie the injury-induced ectopic firing of Aβ-LTMRs? Several studies have reported *de novo* expression of a wide range of pain mediators in large diameter neurons following injury. These include substance P, TRPV1, CGRP, NPY, and other mediators [50, 51, 52, 53, 54, 55, 56, 57]. A recent study by Chen and colleagues provided the first molecular evidence linking SNI-induced mechanical pain to *de novo* transcriptional induction of *npy* gene through mTORC1 activation selectively in large diameter DRG neurons [56]. The authors further showed that selective ablation of mTOR in DRG neurons alleviated SNI-induced mechanical hypersensitivity by suppressing the differential expression of a large set of SNI-responsive genes.

Our proteomic analysis provides the first evidence that LRP1 interacts with phosphatase-related complexes upon TAFA4 stimulation, particularly those involving protein phosphatase 2A (PP2A). The enhanced phosphatase activity observed in DRG cultures following TAFA4 treatment, abolished in *Advillin-LRP1* and *Nav1.8-LRP1* neurons, strongly suggests that TAFA4 modulates neuronal excitability by controlling the phosphorylation/dephosphorylation balance. PP2A is a major regulator of kinase signaling networks, including AKT, ERK, and p70 S6K, all of which converge on mTORC1. This provides a mechanistic link between the observed increase in phosphatase activity and the subsequent decrease in mTORC1 phosphorylation following TAFA4 treatment. Importantly, the TAFA4-induced reduction in phosphorylated mTORC1 and p70 S6K was confined to large-diameter neurons, consistent with the Aβ-LTMR identity of the responding population.

Our findings identify AMPK as a crucial upstream regulator of TAFA4-induced mTORC1 dephosphorylation. TAFA4 stimulation increased AMPK phosphorylation, while pharmacological blockade of AMPK with compound C effectively abolished TAFA4-mediated analgesia in vivo. Given that AMPK is a central metabolic sensor and a potent negative regulator of mTORC1, this pathway likely integrates TAFA4/LRP1 signaling into a broader

cellular energy-regulatory network. It is conceivable that LRP1 activation by TAFA4 triggers a shift in neuronal metabolic state toward reduced anabolic activity, thereby dampening neuronal excitability and synaptic transmission. The genetic validation using *Advillin-TSC2* mice further supports this model: hyperactivation of mTORC1 through *Tsc2* deletion eliminated the analgesic effect of TAFA4, confirming that mTORC1 suppression is both necessary and sufficient for TAFA4-mediated pain relief. The regulation of protein synthesis and metabolism by mTORC1 and AMPK is essential for controlling various cellular processes, including pain mechanisms [58]. AMPK influences protein translation through its downstream kinases by modulating the mTORC1 pathway. In animal models of neuropathy and inflammatory pain, such as chronic constriction injury (CCI), spinal nerve ligation (SNL), and spared nerve injury (SNI), mTORC1 is activated [59]. AMPK inhibits mTORC1 either by directly phosphorylating raptor or by suppressing the tuberous sclerosis complex 2 (TSC2). Notably, mTORC1 and its downstream components are present in 35 to 42% large diameter neurons but only in 3 to 5% of CGRP-positive neurons, and inhibition of mTORC1 increases the thermal threshold of A-fibers, but not C-fibers, and raises the paw withdrawal threshold in animal models of neuropathic pain [56, 60, 61]. This suggests that the mTORC1 pathway in primary sensory neurons plays a pivotal role in maintaining basal sensory function. AMPK also regulates ion channels involved in pain signaling, such as Nav channels and voltage-gated potassium channels. Indeed, the enzyme Nedd4-2, which is regulated by AMPK, controls the ubiquitination and degradation of these channels. In diabetic neuropathy, a reduction in Nedd4-2 causes an increase in the expression of certain Nav channels (Nav1.3, Nav1.7, Nav1.8), which contribute to neuropathic pain [62]. Additionally, AMPK can directly phosphorylate ion channels like KCNQ, TREK and Kv2.1, thereby modulating their activity [63, 64, 65]. In line with this, we recently showed that a 30-minute bath application of TAFA4 was sufficient to fully rescue the SNI-induced alterations in A-type K^+ current (I_A) and in hyperpolarization-activated current (I_h) in the SCDH interneurons

[16]. Furthermore, Chen and colleagues showed that SNI-induced hyperexcitability of nociceptive neurons by Aβ-LTRMs-derived NPY was impaired in mice lacking mTOR selectively in DRG neuron [56]. Based on the above described data, one attractive hypothesis is that TAFA4/LRP1 signaling acts as a disease-modifying drug by indirectly activating AMPK in Aβ-LTMRs. Once activated, phosphorylated AMPK inhibits the mTORC1 pathway leading to a reduction of the injury-induced hypersensitization of Aβ-LTMRs. Desensitized Aβ-LTMRs will reduce the release of NPY within the DRG and at the spinal cord level. At the DRG level, decreased NPY release from Aβ-LTMRs will reduce the NPY-mediated intra-ganglionic activation of nociceptors, which will lead to a reduction in their excitability, resulting in less pain. At the spinal level, decreased release of NPY will decrease the NPY/Y1R-mediated inhibition of spinal cord inhibitory interneurons, decreasing spinal sensitization and restoring efficient spinal inhibition. In line with this, optogenetic activation of Split^{Cre}-Aβ-LTMRs induced c-FOS activation in laminae II inner of the DHSC, and 80% of the activated interneurons were inhibitory interneurons [9].

In summary, our work defines a novel peripheral analgesic mechanism whereby TAFA4 engages LRP1 signaling in Aβ-LTMRs to activate phosphatase complexes, stimulate AMPK, and suppress mTORC1 activity. This cascade ultimately dampens the neuronal activity underlying mechanical hypersensitivity across multiple pain models. These findings establish LRP1 as a critical node in peripheral sensory modulation and identify the TAFA4–LRP1–AMPK/mTORC1 axis as a promising therapeutic target for chronic pain management.

ACKNOWLEGMENTS

We are grateful to the members of the Moqrich lab at IBDM for the scientific discussions. We would like to thanks Elena Brunet for teaching Aude how to do DRG cultures and Pascal Salin for helping for RNAscope experiments. The IBDM imaging and animal facilities for assistance. This work was funded by the FRM-EQP202003010192 grant awarded to A.M. This work was also supported by institutional funding from the CNRS and Aix-Marseille-Université to IBDM. Proteomics analyses were done using the mass spectrometry facility of Marseille Proteomics (marseille-proteomique.univ-amu.fr) supported by IBISA, the Cancéropôle PACA, the Provence-Alpes-Côte d'Azur Region, the Institut Paoli-Calmettes, and Fonds Européen de Développement Regional (FEDER). The electron microscopy experiments were performed on the PiCSL-FBI core facilty (IBDM, AMU-Marseille), member of the France-BioImaging national research infrastructure (ANR-10-INBS-04) and member of the Marseille Imaging Institute, an Excellence Initiative of Aix Marseille University A*MIDEX, a French "Investissements d'Avenir" programme (AMX 19 IET 002).

A.M and F.C designed the project, A.C managed the mouse colonies used in this study, performed the behavioural and all the histological experiments as well as the phosphatase activity assay. She also generated all the figures and managed the writing of the materials and methods section, L.C and S.A performed the proteomic and phosphoprotomeomics experiments and contributed to writing the corresponding chapter. C.S performed all the intrathecal injections, S.G generated the CCI mice and trained A.C for the behavioural experiments, and A.M wrote the manuscript. All authors contributed to editing the manuscript.

AM is the co-founder and CSO of Tafalgie Therapeutics (TT). SG is cofounder and general manager of TT. AC and CS are research scientists of TT. LC, SA, and FC have no conflicts of interest.

DATA AVAILABILITY:

The datasets generated during this study are available from the corresponding author upon reasonable request.

EXPERIMENTAL PROCEDURES

Mice

Mice were maintained under standard housing conditions (22°C, 40% humidity, 12 hr light cycles, and free access to food and water). Mice at 8 to 12 weeks of age and of both sexes were used for experiments. Particular efforts were made to minimize the number of mice used in this study, as well as the stress and suffering to which they were subjected. All experiments were conducted in line with the European guidelines for the care and use of laboratory animals (Council Directive 86/609/EEC).

Ethical Statement

All experimental procedures were approved by an independent ethics committee for animal experimentation (APAFIS), as required by the French law and in accordance with the relevant institutional regulations of French legislation on animal experimentation, under license number 2022020709593954-V4#35163. All experiments were performed in accordance with the ARRIVE guidelines.

Generation of mouse lines

GINIP-DTR mice were obtained by crossing GINIP$^{fl/fl}$ line [13] with mice expressing the CRE recombinase from Nav1.8 locus (*Nav1.8*$^{CRE/+}$ mice). GINIP$^{fl/+}$ Nav1.8$^{cre/+}$ were injected with DT and called GINIP-DTR and GINIP$^{fl/+}$ were used as control.

LRP1$^{fl/fl}$ mice were crossed with *Nav1.8*$^{CRE/+}$, *plp1*$^{CRE\text{-}ert2}$ and *Advillin*$^{CRETg/+}$ (Zurborg et al,. 2011) mice to generate Nav1.8-LPR1, Plp1-LRP1 and Advillin-LRP1. LRP1$^{fl/fl}$ were used as control. Nav1.8$^{-tdTomato}$ and Advillin$^{-tdTomato}$ mice were obtained by crossing *Nav1.8*$^{CRE/+}$ or *Advillin*$^{CRETg/+}$ mice with Rosa26-$^{flx\text{-}Stop\text{-}flxtdTomato}$ mice (B6.Cg-Gt(ROSA)26Sor$^{tm14(CAG\text{-}tdTomato)Hze}$, The Jackson Laboratory, 007914). TSC2 $^{fl/fl}$ mice were crossed with *Advillin*$^{CRETg/+}$ mice to generate Advillin-TSC2.

Experiments with RAP or TAFA4 injections (Fig. 1) and phosphoproteomics experiments, C57/Bl6J mice were purchased from Charles River Laboratories.

Pain models

SNI (Spared Nerve Injury)

The spared nerve injury (SNI) model of peripheral nerve injury was implemented as previously described [66]. Briefly, mice were anesthetized with ketamine (40 mg/kg IP) and xylazine (5 mg/kg, IP) and the left sciatic nerve was exposed under aseptic conditions. The distal trifurcation of the sciatic nerve was identified and the tibial and common peroneal branches were ligated with polypropylene nonabsorbable 6-0 sutures (Ethicon); 1 mm was cut out, leaving the sural branch intact. The wound was closed with sutures, and the animals were allowed to recover and returned to their cages.

Paw incision

Paw incision surgery was performed as described by Brennan [67]. Mice were anesthetized with ketamine (40 mg/kg IP) and xylazine (5 mg/kg IP) and a longitudinal incision was made through the skin and fascia of the right hind paw. Forceps were used to elevate the flexor digitorum brevis muscle longitudinally and an incision was made through the muscle with a scalpel, to cut it into two halves. The wound was closed with sutures, and the animals were allowed to recover and returned to their cages.

CCI (Chronic constriction injury)

Chronic constriction injury was performed by modifying the one described in Bennett et al [66]. In brief, 2 ligatures (6-0 Monocryl, Ethicon) tied loosely (with about 1 mm spacing) around the common sciatic nerve of the right paw were performed on anaesthetized mice (ketamine/xylazine). Nerves were constricted to a barely discernible degree, so that circulation through the epineural vasculature was not interrupted. The wound was closed with sutures.

Animals are kept on a warm chamber and monitored until waking up before returning to their home cage. Weight, general aspect, feeding, and water drinking are verified regularly.

Carrageenan injection

We injected 20 µL of 1% λ -carrageenan (Sigma-Aldrich, 22049-5G-F) in 1 x PBS into the plantar surface of the right hind paw of the mouse with a Hamilton syringe.

Behavioral tests

All behavioral assays were conducted on 8- to 12-week-old mice. Animals were acclimated to their testing environment for 45-60 minutes before each experiment, and all experiments were performed at room temperature (~22°C). Experimenters were blind to the treatments used. Mice of both sexes were used for all experiments.

Von Frey's test

Mice were placed in plastic chambers on a wire mesh grid and stimulated with von Frey filaments (Bioseb) by the up-down method [68] starting with a 1g filament, and using 0.07 and 2g filaments as the cutoffs.

Tail Flick

Mice were immobilized with a tissue and the tip of the tail (1/3 of the length) was immersed in a water bath maintained at 52°C. The latency to nociceptive response (withdrawal of the tail) was measured. To prevent tissue damage, the tail was removed from the bath immediately after a nociceptive response or a cut-off time of 10s respectively. Each mouse was tested three times with a minimum latency of 5 min between each test.

Drugs and *in vivo* administration methods

Synthetic TAFA4 (Genepep) was dissolved in 0.1 M phosphate buffer (PB); baclofen (Sigma-Aldrich) was dissolved in H2O (pH 7.6), SNC80 (Tocris Bioscience) was dissolved in 100 mM HCl; DAMGO (Sigma Aldrich) was dissolved in 0.9 ‰ NaCl; Pregabalin (Sigma) was dissolved in water and RAP (Sigma-Aldrich) was dissolved in 0.9 PB. Drugs were administered

intrathecally (IT) or systemically using subcutaneous (SC) injections in the neck of the mice, as indicated in the figure legends. For IT injections (170 pmol of TAFA4, 160 pmol of RAP, 10 nmol of SNC80, 0.47 nmol of Baclofen or 0.2 nmol of DAMGO), 10 µL of each compound was injected into non-anesthetized mice. Successful placement of the needle was confirmed by a slight flick of the tail. For SC injections (2.6 µM of TAFA4, 2.6 µM of RAP or 2 mM of Pregabalin), 100µl of compound was injected per 10g.

Tamoxifen (T5648, Sigma) was prepared in corn oil and was injected per os in both, control and Plp1-LRP1 mice, for 5 consecutive days at 200mg/kg to 6 old weeks mice.

For RTX treatment, 4 weeks old C57/Bl6J mice purchased from Charles River Laboratories received injections of RTX in the flank for 3 days with increasing doses (30-70-100 µg/kg). RTX (AG-CN2-0534, Adipogen) was prepared in DMSO and diluted in PBS. Control mice were treated with PBS only.

Diphtheria Toxin (Sigma Aldrich) (20 µg/kg) was injected i.p. on 2 days; separated by 72 h on 4 weeks old GINIP-DTR mice. Behavioral tests were performed 4 weeks after the initial DT injection.

Primary sensory neurons culture preparation

All DRGs were carefully extracted and digested with 2mg/mL of collagenase type II (GIBCO), 5mg/mL of dispase (GIBCO) and 5mM of CaCl2 (Honeywell) in HBSS media (magnesium- and calcium- free) containing 5mM HEPES, 10mM D-Glucose and 1% penicillin/streptomycin, at pH 7.5 for 1h at 37°C. After removing the supernatant, DRGs were resuspended with Leibovitz-15 complete medium (L-15 supplemented with 5% FCS and 1% penicillin/streptomycin), and then mechanically dissociated with two glass Pasteur pipettes of decreasing diameter (1 and 0.5 mm). The resulting suspensions were subjected to a density gradient centrifugation through Percoll (onto 12.5 and 28% Percoll gradient in Leibovitz-15 complete medium) at a speed of 1300g (acc=6, break=3) for 20 minutes, to eliminate cell debris.

Cells were washed with Leibovitz-15 complete medium and speed at 900g (acc=7, break=8) for 5 minutes. Cells were then resuspended in Neurobasal complete medium (Neurobasal A medium supplemented with 2mM L-glutamine, 1% penicillin/streptomycin and B27 1X) containing the following factors: Nerve growth factor (NGF) at 50ng/mL, Glial cell-derived neurotrophic factor (GDNF) at 50ng/mL, Neurotrophin-3 (NT3) at 50ng/mL, Neurotrophin-4 (NT4) at 10ng/mL and Brain Derived Neurotrophic Factor (BDNF) at 5ng/mL.

For immunostaining, cover glass (diameter of 13 mm, thickness No. 1.5, VWR) were put on 24 wells cell culture plates and coated 1 hour with Poly-D-lysine (50 µg/ml) and 2 hours with Laminin (10 µg/ml) at 37°C. Then, cell suspension was plated on the cover glass. After 24h, cells were washed with PBS and fixed 15 minutes with PAF 4% (in PBS).

For samples for phosphatase activity and phosphoproteomics analysis, 24 wells cell culture plates were coated 1 hour with Poly-D-lysine (50 µg/ml) and 2 hours with Laminin (10 µg/ml) at 37°C. Then, cell suspension was plated in the wells (1 mouse=1 well). After 24 hours, DRG cultures were stimulated.

Stimulation of DRG cultures and phosphatase activity

After 24 hours in culture, cells were stimulated with or without 50 nM of TAFA4 in Neurobasal A medium at 37°C. Then, cells were washed with PBS 1X and lysed with 333 µl per well with a lysis buffer (for 50 mL total: 100mM NaCl, 2mM EDTA, 50 nM Tris HCl pH 8.3, 1% NP40 and the Roche cOmplete EDTA-free protease inhibitor cocktail). For phosphoproteomics analysis, 3 mice were pooled to make one sample. Then, cell lysates were centrifuged 10 min at 13 000 rpm at 5°C. Phosphatase activity of cell lysates was measured in 96 wells plate (GREINER, ref 675096) using Clariostar Plus – Star Control (BMG Labtech). 22µl of a mix (BSA at 0,5 mg/ml (Sigma), NiCl at 4,5 mM (Sigma, 339350), TrisHCl pH 7.0 at 40 mM) were added to 18µL of cell lysate. Extemporaneously, 60µl of diFMUP (200µM diluted in TrisHCl pH 7.0 at 50 mM, Tocris, ref 6882) were added in each well before to read the plate with

excitation at 358 nm and emission at 452 nm for 30 minutes. The slope of the curve give access to phosphatase activity.

Histology

Tissue processing for immunofluorescence (IF)

Mice were deeply anesthetized with a mix of ketamine/xylazine and then intracardially perfused with 0.1 M phosphate buffer (PB) followed by an ice-cold solution of paraformaldehyde 4% in 0.1 M PB (4% PFA).

DRGs were dissected and further fixed for 12h in ice-cold 4% PFA before to be transferred into a 30% (w/v) sucrose solution for cryoprotection and incubated at 4°C until they sank. They were then frozen in OCT mounting medium and stored at −80 °C. 14µm cryosections were obtained using a standard cryostat (Leica). These sections were mounted on Superfrost slides and kept at -80°C until their use for IF experiments.

For teased nerve, sciatic nerves were dissected and cut into small pieces. Using a pair of fine forceps, they were separated into smaller fiber bundles from which single fibers are isolated. The work is performed on Superfrost slides. Then, slides are dried and put at -80°C. Before the saturation, tissues are fixed for 20 minutes in a mix methanol/acetone (v/v).

Immunostaining

All tissues/cells were washed for 5 minutes (min) in PBS and then incubated for 1 h at room temperature (RT) with a blocking solution (10% donkey serum (Sigma), 3% BSA (Sigma), 0.4% Triton X-100, in PBS) and incubated overnight at 4°C with primary antibodies diluted in the same blocking solution. After three washes with PBS, tissues/cells were incubated for 1 h at RT with secondary antibodies diluted in the blocking solution describe above. Tissues were washed again 3 times in PBS before being mounted with ImmuMount Reagent (Thermo Scientific). Cells and teased nerve were previously stained for 15 min with Hoechst (1:5000, Invitrogen, 33342). Images were acquired with a Zeiss AxioImager M2 fluorescence

microscope with a 10x, 20x or x63 objectives and appropriate excitation wavelengths and emission filters. Acquisition settings were kept constant between image acquisitions for different conditions. Images were analyzed with ImageJ software.

Immunostainings were done with rabbit anti-TH (1:500, Sigma-Aldrich AB152), goat anti-CGRP (1:500, OriGene, BP022); rabbit anti LRP1 C-ter (1:1000, Abcam, #ab92544), rat anti-RFP (1:1000, Chromotek, 5F8); goat anti Ret (1:150, R&D Systems, AF482); goat anti-TrkC (1:1000, R&D Systems, AF1404); rabbit anti-PV (1:1000, SWant, PV27); rabbit anti-neurofilament M (145 kDa) (1:1000, Sigma-Aldrich, AB1987); mouse anti-β tubulin III (1:1000, Sigma, T8660), rabbit mTOR (1:1000, Cell signaling, 2972); rabbit phosphor-mTOR Serine 2448 (1:1000, Cell signaling, 2971).

Secondary antibodies were donkey anti-rabbit, anti-rat and anti-goat antibodies conjugated to Alexa Fluor 488, 555, or 647 (1:500, Thermo Fisher Scientific). Isolectin binding 4 (IB4) conjugated to Alexa Fluor 647 was used at a dilution of 1:500 (Thermo Fisher Scientific, #I32450).

RNAscope

In situ hybridization was performed using the RNAscope 2.5 HD Detection Reagent - RED kit (Advanced Cell Diagnostics) with 15 min post-fixing with 4% paraformaldehyde (PFA) in phosphate buffered saline (PBS) at 4°C and stepwise dehydration with 70%, 95% and 100% ethanol at RT. The slides were dried briefly and then boundaries were drawn around each section using a hydrophobic pen (ImmEdge PAP pen; Vector Labs). Tissue pre-treatment consisted of hydrogen peroxide (10 min at RT) and protease III (30 min at 40°C). Following pre-treatment, probe hybridization using Mm-Lrp1 probe (ACD Probe Cat No. 465231) and detection were performed according to the manufacturer's protocol. Slides were finally processed for immunohistochemistry (as previously described) with rabbit anti-PGP9.5 antibody (1:750, ThermoFisher, PA5-29012).

Electron microscopy

Plp1-LRP1 mice (n=5 cre+; n=3 cre-) were deeply anesthetized with a mix of ketamine/xylazine and then intracardially perfused with 0.1 M phosphate buffer (PB) followed by a mix of PFA 2% and glutaraldehyde 2.5 % in 0.1M PB. Sciatic nerves were dissected out, post fixed for 2h in the same aldehyde mixture and washed in PB. Transversal sections were cut on a vibratome (Leica VT1000S) at a thickness of 80 µm. Nerve sections were punched out (1.5 mm diameter) and frozen with BSA 20% using Leica EM Pact2 high pressure freezer. After freezing, samples were freeze-substituted at -90°C in tannic acid containing 0.1% of acetone during 96 hours. Then, they were washed in acetone and put in 2% OsO4/0.1% uranyl in acetone for 7 hours. The temperature was gradually increased to -20°C and maintained for 14 hours, before to be raised to 4°C for 24h. Samples were finally washed in acetone and embedded with EPON resin. Resin was polymerized at 60 °C for 48 hours. 90 nm ultrathin sections were performed and placed on cooper grid using an ultramicrotome (Leica UC7). Sections were further counterstained with 2% uranyl acetate and Lead citrate before to be image with Tecnai G2 microscope (FEI) at 200kV and acquire with a Veleta camera (Olympus, Japan).

Proteome analysis

Protein Lysates were loaded on NuPAGE™ 4–12% Bis–tris acrylamide gels according to the manufacturer's instructions (Life Technologies). Running of protein was stopped as soon as proteins stacked in a single band. Protein containing bands were stained with Imperial Blue (Pierce), cut from the gel and digested with high sequencing grade trypsin (Promega) before mass spectrometry analysis. Briefly, gel pieces were washed and destained using few steps of 100mM NH4HCO3. Destained gel pieces were shrunk with 100 mM ammonium bicarbonate in 50% acetonitrile and dried at RT. Protein spots were then rehydrated using 10mM DTT in 25 mM ammonium bicarbonate pH 8.0 for 45 min at 56°C. This solution was replaced by 55 mM iodoacetamide in 25 mM ammonium bicarbonate pH 8.0 and the gel pieces were incubated

for 30 min at room temperature in the dark. They were then washed twice in 25 mM ammonium bicarbonate and finally shrunk by incubation for 5 min with 25 mM ammonium bicarbonate in 50% acetonitrile. The resulting alkylated gel pieces were dried at RT. The dried gel pieces were reswollen by incubation in 25 mM ammonium bicarbonate pH 8.0 supplemented with 12.5 ng/µl trypsin (Promega) for 1h at 4°C and then incubated overnight at 37°C. Peptides were harvested by collecting the initial digestion solution and carrying out two extractions; first in 5% formic acid and then in 5% formic acid in 60% acetonitrile. Pooled extracts were dried down in a centrifugal vacuum system. Samples were reconstituted in 0.1% TFA 4% acetonitrile before mass spectrometry using an Orbitrap Fusion Lumos Tribrid Mass Spectrometer (ThermoFisher Scientific, San Jose, CA) online with an Ultimate 3000RSLCnano chromatography system (ThermoFisher Scientific, Sunnyvale, CA). Peptides were separated at 40°C using a two steps linear gradient (4–20% acetonitrile/H2O; 0.1% formic acid for 110 min and 20-32% acetonitrile/H2O; 0.1% formic acid for 10 min). An EASY-Spray nanosource was used for peptide ionization (2,200 V, 275°C). MS was conducted using a data-independent acquisition mode (DIA). Full MS scans were acquired in the range of m/z 375–1,500 at a resolution of 120,000 at m/z 200 and the automatic gain control (AGC) was set at 4.0 × 10E5 with a 50 ms maximum injection time. MS2 spectra were acquired in the Orbitrap with a resolution of 30,000, in the mass range of 200-1800 m/z after isolation of parent ion in the quadrupole and fragmentation in the HCD cell under collision Energy of 30%. DIA parent ion range was from 400 to 1000 m/z divided into 40 windows 16 Da wide and from 1000 to 1500 m/z divided into 10 windows 50 Da wide.

For protein identification and quantification, relative intensity-based label-free quantification (LFQ) was processed using the DIA-NN 1.8 algorithm (Demichev et al, 2020). Raw files were searched against the mouse database from UniProt (UP000000589, 55341 entries, 2022/02/24) implemented with a contaminant database (Frankenfield et al JPR 2022). The following

parameters were used for searches: (i) trypsin allowing cleavage before proline; (ii) one missed cleavage was allowed; (iii) cysteine carbamidomethylation (+57.02146) as a fixed modification and methionine oxidation (+15.99491) and N-terminal acetylation (+42.0106) as variable modifications; (iv) a maximum of 1 variable modification per peptide allowed; and (v) minimum peptide length was 7 amino acids and a maximum of 30 amino acids. The match between runs option was enabled. The precursor false discovery was set to 1%. DIA-NN parameters were set on double-pass mode for Neural Network classifier, Robust LC High precision for quantification strategy and RT-dependent mode for Cross-run normalization. Library was generated using Smart profiling set up. The mass spectrometry proteomics data have been deposited to the ProteomeXchange Consortium via the PRIDE partner repository with the data set identifier PXDxxxxx (Perez-Riverol et al., 2019). Main output file from DIA-NN was further filtered at 1% FDR and LFQ intensity was calculated using our DIAgui package at 1% q-value (https://github.com/marseille-proteomique/DIAgui [69]). The statistical analysis was done with Perseus software (version 1.6.15.0), where proteins were pre-filtered to remove contaminants, and those with less than 70% valid quantitative values across treatment groups. Missing values were then imputed using Perseus's normal distribution imputation method (Width: 0.3, Down shift: 1.8). Differential proteins were assessed using a two-sample t test with a permutation-based false discovery rate of 0.05, employing 250 iterations and the parameter So set to 0.1 (Tyronova and Cox, 2018).

Affinity purification mass spectrometry analysis

Pre-cleared lysate from brain plasma membrane were incubate with Anti-HA-magnetic beads pre-loaded with synthetic HA-TAFA4 or BSA as control. Beads were eluted on ice with 0.1M Glycine pH=2. Samples were then loaded on NuPAGE™ 4–12% Bis–tris acrylamide gels and processed as mentioned above for Proteome analysis. Samples were injected as above on the same mass spectrometer, however MS was conducted using a data-dependant acquisition mode

(DDA). Peptides were separated on a Thermo Scientific Acclaim PepMap RSLC C18 column (2 µm, 100A, 75 µm × 50 cm). For peptide ionization in the EASY-Spray nanosource in front of the Orbitrap Fusion Lumos Tribrid Mass Spectrometer, spray voltage was set at 2.2 kV and the capillary temperature at 275 °C. The Orbitrap Lumos was used in data-dependent mode to switch consistently between MS and MS/MS. The time between master scans was set to 3 seconds. MS spectra were acquired with the Orbitrap in the range of m/z 400–1600 at a FWHM resolution of 120,000 measured at 400 m/z. AGC target was set at 4.0e5 with a 50 ms maximum injection time. For internal mass calibration, the 445.120025 ions were used as lock mass. The more abundant precursor ions were selected, and collision induced dissociation fragmentation was performed in the ion trap to have maximum sensitivity and yield a maximum amount of MS/MS data. Number of precursor ions was automatically defined along run in 3 s windows using the ―Inject Ions for All Available parallelizable time option‖ with a maximum injection time of 300 ms. The signal threshold for an MS/MS event was set to 5,000 counts. Charge state screening was enabled to exclude precursors with 0 and 1 charge states. Dynamic exclusion was enabled with a repeat count of 1 and duration of 60 s.

Relative intensity-based label-free quantification (LFQ) was processed using the MaxLFQ algorithm from the freely available MaxQuant computational proteomics platform, version 1.6.3.4 (Tyanova et al 2016). Spectra were searched against the mouse proteome extracted from UniProt on the 15 April 2021, which produced 55,470 entries (UP000000589 Mus musculus (Mouse) (C57BL/6J)). The false discovery rate (FDR) at the peptide and protein levels were set to 1% and determined by searching a reverse database. For protein grouping, all proteins that could not be distinguished on the basis of their identified peptides were assembled into a single entry according to the MaxQuant rules. Statistical analysis was done with Perseus program (version 1.6.15.0) from the MaxQuant environment (www.maxquant.org) (Tyanova and Cox, 2018). Quantifiable proteins were defined as those detected in above 70% of samples in one

condition or more. To obtain a normal distribution, protein LFQ normalized intensities transformed using base 2 logs. Missing values were replaced using data imputation by randomly selecting from a normal distribution centred on the lower edge of the intensity values that simulates signals of low abundant proteins using default parameters (a downshift of 1.8 standard deviation (s.d.) and a width of 0.3 of the original distribution). To determine whether a given detected protein was specifically differential, a two-sample t-test was done using permutation-based FDR-controlled at 0.01 and employing 250 permutations. The p value was adjusted using a scaling factor s0 with a value of 1. Analysis was done on biological triplicates, each run three times on mass spectrometers. The mass spectrometry proteomics data have been deposited to the ProteomeXchange Consortium via the PRIDE (Reference Perez-Riverol Nucleix Acids 2019) partner repository with the dataset identifier PXDzzzzzzz.

Phosphoproteome analysis

100mg of protein lysates per condition were used and adjusted to 100ml with 100mM triethyl ammonium bicarbonate (TEAB) and reduced using 5ml of 200mM (TCEP) in 100mM TEAB at 55°C for 1 hour. Then samples were alkylated using 5ml of 375mM iodoacetamide in 100mM TEAB at room temperature for 30 minutes. Proteins were then precipitated using 6 volumes of acetone at -20°C overnight. Resuspended protein pellets in 100ml of 100mM TEAB were digested overnight using 2.5mg of trypsin. Tryptic peptides were labelled using a Tandem Mass Tag (TMT) TMT-16plex isobaric label reagent set (ThermoFisher Scientific, San Jose, CA) following the manufacturer's instructions and combined into one 16-plex sample (Thompson et al., 2019). The pooled sample were then desalted on a C18 classic Sep-Pak cartridge (Waters) and divided in 4 equal amount. Phosphopeptide enrichment was performed manually using MagReSyn beads (ReSyn Biosciences). Four different enrichment were done using respectively MagReSyn-Tio2, MagReSyn-ZrO2, MagReSyn TI-IMAC HP and MagReSyn Zr-IMAC HP using product instruction guide. The four enrichment were then pooled together before mass

spectrometry analysis using an Orbitrap Fusion Lumos Tribrid Mass Spectrometer (ThermoFisher Scientific, San Jose, CA) online with an Ultimate 3000RSLCnano chromatography system (ThermoFisher Scientific, Sunnyvale, CA). Peptides were separated at 40°C using a two steps linear gradient (2–22% acetonitrile/H2O; 0.1% formic acid for 200 min and 22-36% acetonitrile/H2O; 0.1% formic acid for 10 min). An EASY-Spray nanosource was used for peptide ionization (1,900 V, 275°C). The mass spectrometer was used in data dependent mode to switch consistently between MS1, MS2 for peptide identification and quantification protein. Time between Masters Scans was set to 3 seconds. MS1 spectra were acquired with the Orbitrap in the range of m/z 400-1600 at a FWHM resolution of 120 000 measured at 200 m/z. AGC target was set at standard with an auto maximum injection time. The more abundant precursor ions were selected for MS2 and fragmented by stepped HCD followed by orbitrap analysis at 15, 30 and 45% collision energy (Resolution = 50 000; First mass = 120 m/z; AGC target = custom; MaxIT = custom). Charge state screening was enabled to include precursors with 2 and 6 charge states. Dynamic exclusion was enabled with a repeat count of 1 and a duration of 60s. The mass spectrometry proteomics data have been deposited to the ProteomeXchange Consortium via the PRIDE partner repository with the data set identifier PXDxxxxx [70].

Raw files generated from mass spectrometry analysis were processed to identified and quantified peptides from MS2 spectrum using MaxQuant (Tyanova et al 2016) (Max Planck Institute, www.maxquant.org, version 2.4.2.0) database search against Mouse Database from the UniProt database (UP000000589, 55341 entries, 2022/02/24) supplemented with a set of frequently observed contaminants. The search was done using mainly default parameters with a parent ion tolerance of 4.5 ppm, a fragment ion tolerance of 20 ppm, and a reporter ion tolerance of 0.003 Da (Reporter Ion Isotopic Distributions for Lot WC319900 was used). Carbamidomethylation on cysteine (+57.021 Da) and TMTpro16Plex tags on N termini as well

as lysine (+304.207 Da) were set as static modifications. Dynamic modifications included oxidation on methionine (+15.995 Da) and acetylation on N-term (+42.011). The false discovery rate (FDR) at the peptide and protein levels were set to 1% and determined by searching a reverse database. The statistical analysis was done with Perseus program (version 1.6.15.0) (Tyanova S et al. Methods Mol Biol 2018). The differential phosphopeptides analysis was carried out on after removal of peptides from contaminant database. Peptide TMT corrected intensities were base 2 logarithmized to obtain a normal distribution and normalized by subtracting the median. Missing values were replaced using data imputation by randomly selecting from a normal distribution to simulate signals of low abundant peptides using default parameters (a downshift of 1.8 standard deviation and a width of 0.3 of the original distribution). To determine whether a given detected phosphopeptide was specifically differential, a two-sample t-test was done using permutation-based FDR-controlled at 0.05 and employing 250 permutations.

Quantification and statistical analysis

Results were expressed as mean +/- SEM. Quantitative and statistical analyses were performed by using the GraphPad Prism 7 (GraphPad Software, La Jolla, CA) and were indicated in each figure. Statistical significance was set to *P , 0.05, **P , 0.01,***P , 0.001, and ****P , 0.0001.

REFERENCES

1. Finnerup NB, Kuner R, Jensen TS. Neuropathic Pain: From Mechanisms to Treatment. *Physiological reviews* **101**, 259-301 (2021).

2. Abraira VE, Ginty DD. The sensory neurons of touch. *Neuron* **79**, 618-639 (2013).

3. Abraira VE*, et al.* The Cellular and Synaptic Architecture of the Mechanosensory Dorsal Horn. *Cell* **168**, 295-310 e219 (2017).

4. Dubin AE, Patapoutian A. Nociceptors: the sensors of the pain pathway. *J Clin Invest* **120**, 3760-3772 (2010).

5. Li L*, et al.* The functional organization of cutaneous low-threshold mechanosensory neurons. *Cell* **147**, 1615-1627 (2011).

6. Melzack R, Wall PD. Pain mechanisms: a new theory. *Science* **150**, 971-979 (1965).

7. Arcourt A*, et al.* Touch Receptor-Derived Sensory Information Alleviates Acute Pain Signaling and Fine-Tunes Nociceptive Reflex Coordination. *Neuron* **93**, 179-193 (2017).

8. Cui L*, et al.* Identification of Early RET+ Deep Dorsal Spinal Cord Interneurons in Gating Pain. *Neuron* **91**, 1413 (2016).

9. Gautam M*, et al.* Distinct local and global functions of mouse Abeta low-threshold mechanoreceptors in mechanical nociception. *Nat Commun* **15**, 2911 (2024).

10. Tashima R*, et al.* Optogenetic Activation of Non-Nociceptive Abeta Fibers Induces Neuropathic Pain-Like Sensory and Emotional Behaviors after Nerve Injury in Rats. *eNeuro* **5**, (2018).

11. Chamessian A*, et al.* Is Optogenetic Activation of Vglut1-Positive Abeta Low-Threshold Mechanoreceptors Sufficient to Induce Tactile Allodynia in Mice after Nerve Injury? *J Neurosci* **39**, 6202-6215 (2019).

12. Delfini MC*, et al.* TAFA4, a chemokine-like protein, modulates injury-induced mechanical and chemical pain hypersensitivity in mice. *Cell Rep* **5**, 378-388 (2013).

13. Gaillard S*, et al.* GINIP, a Galphai-interacting protein, functions as a key modulator of peripheral GABAB receptor-mediated analgesia. *Neuron* **84**, 123-136 (2014).

14. Kambrun C, Roca-Lapirot O, Salio C, Landry M, Moqrich A, Le Feuvre Y. TAFA4 Reverses Mechanical Allodynia through Activation of GABAergic Transmission and Microglial Process Retraction. *Cell Rep* **22**, 2886-2897 (2018).

15. Reynders A*, et al.* Gut microbiota promotes pain chronicity in Myosin1A deficient male mice. *Brain Behav Immun* **119**, 750-766 (2024).

16. Yoo S*, et al.* TAFA4 relieves injury-induced mechanical hypersensitivity through LDL receptors and modulation of spinal A-type K(+) current. *Cell Rep* **37**, 109884 (2021).

17. Clerc N, Moqrich A. Diverse roles and modulations of I(A) in spinal cord pain circuits. *Cell Rep* **38**, 110588 (2022).

18. Herz J, Strickland DK. LRP: a multifunctional scavenger and signaling receptor. *J Clin Invest* **108**, 779-784 (2001).

19. Xing P*, et al.* Roles of low-density lipoprotein receptor-related protein 1 in tumors. *Chin J Cancer* **35**, 6 (2016).

20. Olbromski M*, et al.* Prognostic significance of alpha-2-macrglobulin and low-density lipoprotein receptor-related protein-1 in various cancers. *Am J Cancer Res* **14**, 3036-3058 (2024).

21. Lin L, Hu K. LRP-1: functions, signaling and implications in kidney and other diseases. *Int J Mol Sci* **15**, 22887-22901 (2014).

22. Potere N, Del Buono MG, Mauro AG, Abbate A, Toldo S. Low Density Lipoprotein Receptor-Related Protein-1 in Cardiac Inflammation and Infarct Healing. *Front Cardiovasc Med* **6**, 51 (2019).

23. Wujak L, Schnieder J, Schaefer L, Wygrecka M. LRP1: A chameleon receptor of lung inflammation and repair. *Matrix Biol* **68-69**, 366-381 (2018).

24. Calvier L, Herz J, Hansmann G. Interplay of Low-Density Lipoprotein Receptors, LRPs, and Lipoproteins in Pulmonary Hypertension. *JACC Basic Transl Sci* **7**, 164-180 (2022).

25. Garcia-Fernandez P, Uceyler N, Sommer C. From the low-density lipoprotein receptor-related protein 1 to neuropathic pain: a potentially novel target. *Pain Rep* **6**, e898 (2021).

26. Wohlford GF*, et al.* A phase 1 clinical trial of SP16, a first-in-class anti-inflammatory LRP1 agonist, in healthy volunteers. *PLoS One* **16**, e0247357 (2021).

27. Brifault C, Kwon H, Campana WM, Gonias SL. LRP1 deficiency in microglia blocks neuro-inflammation in the spinal dorsal horn and neuropathic pain processing. *Glia* **67**, 1210-1224 (2019).

28. Gonias SL, Campana WM. LDL receptor-related protein-1: a regulator of inflammation in atherosclerosis, cancer, and injury to the nervous system. *Am J Pathol* **184**, 18-27 (2014).

29. Orita S*, et al.* Schwann cell LRP1 regulates remak bundle ultrastructure and axonal interactions to prevent neuropathic pain. *J Neurosci* **33**, 5590-5602 (2013).

30. Rohlmann A, Gotthardt M, Hammer RE, Herz J. Inducible inactivation of hepatic LRP gene by cre-mediated recombination confirms role of LRP in clearance of chylomicron remnants. *J Clin Invest* **101**, 689-695 (1998).

31. Zurborg S*, et al.* Generation and characterization of an Advillin-Cre driver mouse line. *Mol Pain* **7**, 66 (2011).

32. Stirling LC*, et al.* Nociceptor-specific gene deletion using heterozygous NaV1.8-Cre recombinase mice. *Pain* **113**, 27-36 (2005).

33. Usoskin D*, et al.* Unbiased classification of sensory neuron types by large-scale single-cell RNA sequencing. *Nat Neurosci* **18**, 145-153 (2015).

34. Tyanova S, Temu T, Cox J. The MaxQuant computational platform for mass spectrometry-based shotgun proteomics. *Nat Protoc* **11**, 2301-2319 (2016).

35. Tyanova S, Cox J. Perseus: A Bioinformatics Platform for Integrative Analysis of Proteomics Data in Cancer Research. *Methods Mol Biol* **1711**, 133-148 (2018).

36. Reynhout S, Janssens V. Physiologic functions of PP2A: Lessons from genetically modified mice. *Biochim Biophys Acta Mol Cell Res* **1866**, 31-50 (2019).

37. Thompson JW*, et al.* International Ring Trial of a High Resolution Targeted Metabolomics and Lipidomics Platform for Serum and Plasma Analysis. *Anal Chem* **91**, 14407-14416 (2019).

38. Gwinn DM*, et al.* AMPK phosphorylation of raptor mediates a metabolic checkpoint. *Molecular cell* **30**, 214-226 (2008).

39. Sancak Y*, et al.* PRAS40 is an insulin-regulated inhibitor of the mTORC1 protein kinase. *Molecular cell* **25**, 903-915 (2007).

40. Han HC, Lee DH, Chung JM. Characteristics of ectopic discharges in a rat neuropathic pain model. *Pain* **84**, 253-261 (2000).

41. Khan GM, Chen SR, Pan HL. Role of primary afferent nerves in allodynia caused by diabetic neuropathy in rats. *Neuroscience* **114**, 291-299 (2002).

42. Li Y, Dorsi MJ, Meyer RA, Belzberg AJ. Mechanical hyperalgesia after an L5 spinal nerve lesion in the rat is not dependent on input from injured nerve fibers. *Pain* **85**, 493-502 (2000).

43. Sun Q, Tu H, Xing GG, Han JS, Wan Y. Ectopic discharges from injured nerve fibers are highly correlated with tactile allodynia only in early, but not late, stage in rats with spinal nerve ligation. *Exp Neurol* **191**, 128-136 (2005).

44. Ruscheweyh R, Forsthuber L, Schoffnegger D, Sandkuhler J. Modification of classical neurochemical markers in identified primary afferent neurons with Abeta-, Adelta-, and C-fibers after chronic constriction injury in mice. *J Comp Neurol* **502**, 325-336 (2007).

45. Campbell JN, Raja SN, Meyer RA, Mackinnon SE. Myelinated afferents signal the hyperalgesia associated with nerve injury. *Pain* **32**, 89-94 (1988).

46. Ossipov MH, Bian D, Malan TP, Jr., Lai J, Porreca F. Lack of involvement of capsaicin-sensitive primary afferents in nerve-ligation injury induced tactile allodynia in rats. *Pain* **79**, 127-133 (1999).

47. Shir Y, Seltzer Z. A-fibers mediate mechanical hyperesthesia and allodynia and C-fibers mediate thermal hyperalgesia in a new model of causalgiform pain disorders in rats. *Neurosci Lett* **115**, 62-67 (1990).

48. Urien L*, et al.* Genetic ablation of GINIP-expressing primary sensory neurons strongly impairs Formalin-evoked pain. *Sci Rep* **7**, 43493 (2017).

49. Abrahamsen B*, et al.* The cell and molecular basis of mechanical, cold, and inflammatory pain. *Science* **321**, 702-705 (2008).

50. Noguchi K, Kawai Y, Fukuoka T, Senba E, Miki K. Substance P induced by peripheral nerve injury in primary afferent sensory neurons and its effect on dorsal column nucleus neurons. *J Neurosci* **15**, 7633-7643 (1995).

51. Hudson LJ, Bevan S, Wotherspoon G, Gentry C, Fox A, Winter J. VR1 protein expression increases in undamaged DRG neurons after partial nerve injury. *The European journal of neuroscience* **13**, 2105-2114 (2001).

52. Nitzan-Luques A, Devor M, Tal M. Genotype-selective phenotypic switch in primary afferent neurons contributes to neuropathic pain. *Pain* **152**, 2413-2426 (2011).

53. Weissner W, Winterson BJ, Stuart-Tilley A, Devor M, Bove GM. Time course of substance P expression in dorsal root ganglia following complete spinal nerve transection. *The Journal of comparative neurology* **497**, 78-87 (2006).

54. Elbaz B*, et al.* Sensory neurons display cell-type-specific vulnerability to loss of neuron-glia interactions. *Cell Rep* **40**, 111130 (2022).

55. Renthal W*, et al.* Transcriptional Reprogramming of Distinct Peripheral Sensory Neuron Subtypes after Axonal Injury. *Neuron* **108**, 128-144 e129 (2020).

56. Chen L*, et al.* mTOR-neuropeptide Y signaling sensitizes nociceptors to drive neuropathic pain. *JCI Insight* **7**, (2022).

57. Sharma N, Flaherty K, Lezgiyeva K, Wagner DE, Klein AM, Ginty DD. The emergence of transcriptional identity in somatosensory neurons. *Nature* **577**, 392-398 (2020).

58. Price TJ, Dussor G. AMPK: An emerging target for modification of injury-induced pain plasticity. *Neurosci Lett* **557 Pt A**, 9-18 (2013).

59. Wang S, Dai Y. Roles of AMPK and Its Downstream Signals in Pain Regulation. *Life (Basel)* **11**, (2021).

60. Geranton SM, *et al.* A rapamycin-sensitive signaling pathway is essential for the full expression of persistent pain states. *J Neurosci* **29**, 15017-15027 (2009).

61. Jimenez-Diaz L, *et al.* Local translation in primary afferent fibers regulates nociception. *PLoS One* **3**, e1961 (2008).

62. Laedermann CJ, *et al.* Dysregulation of voltage-gated sodium channels by ubiquitin ligase NEDD4-2 in neuropathic pain. *J Clin Invest* **123**, 3002-3013 (2013).

63. Andersen MN, Rasmussen HB. AMPK: A regulator of ion channels. *Commun Integr Biol* **5**, 480-484 (2012).

64. Kreneisz O, Benoit JP, Bayliss DA, Mulkey DK. AMP-activated protein kinase inhibits TREK channels. *The Journal of physiology* **587**, 5819-5830 (2009).

65. Ikematsu N, *et al.* Phosphorylation of the voltage-gated potassium channel Kv2.1 by AMP-activated protein kinase regulates membrane excitability. *Proceedings of the National Academy of Sciences of the United States of America* **108**, 18132-18137 (2011).

66. Bennett GJ, Xie YK. A peripheral mononeuropathy in rat that produces disorders of pain sensation like those seen in man. *Pain* **33**, 87-107 (1988).

67. Brennan TJ. Postoperative Models of Nociception. *ILAR J* **40**, 129-136 (1999).

68. Chaplan SR, Bach FW, Pogrel JW, Chung JM, Yaksh TL. Quantitative assessment of tactile allodynia in the rat paw. *Journal of neuroscience methods* **53**, 55-63 (1994).

69. Gerault MA, Camoin L, Granjeaud S. DIAgui: a Shiny application to process the output from DIA-NN. *Bioinform Adv* **4**, vbae001 (2024).

70. Perez-Riverol Y, *et al.* Quantifying the impact of public omics data. *Nat Commun* **10**, 3512 (2019).

FIGURE LEGENDS

Figure 1. TAFA4 acts through LRP1 in sensory neurons

(A–C) Paw withdrawal thresholds in response to static mechanical stimulation (von Frey assay) were measured on the ipsilateral and contralateral (dotted line) paws before (baseline) and one day after paw incision. **(A)** Intrathecal (IT) administration of TAFA4 (170 pmol = 2 mg/kg, black line), either alone or in combination with RAP (170 pmol, grey line). **(B)** Subcutaneous (SC) administration of TAFA4 (770 pmol = 300 µg/kg, black line), with or without co-administration of RAP (770 pmol, grey line). **(C)** SC administration of TAFA4 (770 pmol, black line) with or without IT RAP (170 pmol, grey line). **(D)** Schematic diagram illustrating the strategy to generate *Plp1-LRP1* and control mice, and the tamoxifen treatment protocol used to induce CRE-mediated recombination. **(E, F, H, I)** Paw withdrawal thresholds were assessed on the ipsilateral paw before (baseline) and 7 days after spared nerve injury (SNI). **(E)** SC injection of TAFA4 restored mechanical thresholds 2 hours post-injection in both control and *Plp1-LRP1* (E). **(F)** IT injection of TAFA4 also significantly increased the withdrawal threshold in both genotypes. **(G)** Schematic diagram of the strategy used to generate *Advillin-LRP1* and control mice. **(H)** SC administration of TAFA4 significantly increased withdrawal thresholds 2 hours post-injection in control mice but not in *Advillin-LRP1* mice. **(I)** IT injection of TAFA4 increased mechanical thresholds in both control and *Advillin-LRP1* mice. **(J–L)** TAFA4 significantly increased paw withdrawal thresholds in the ipsilateral paw of control mice, but not in *Advillin-LRP1* mice, in the following pain models: **(J)** Paw incision (Brennan model), **(K)** Carrageenan-induced inflammation, and **(L)** Chronic constriction injury (CCI). All data are presented as mean ± SEM. Statistical significance was determined using two-way repeated measures ANOVA followed by Bonferroni post hoc tests. The number of mice per condition is indicated in parentheses.

Figure 2. TAFA4 acts through LRP1 in Aβ-LTMRs

(A, D, G) Schematic representations of the strategies used to generate: **(A)** *Nav1.8-LRP1* and control mice, **(D)** *GINIP-DTR* and *GINIP^fl/+* mice, and **(G)** RTX-treated mice. Panels **(D)** and **(G)** also illustrate the experimental designs for diphtheria toxin (DT) and resiniferatoxin (RTX) treatments, respectively. **(B, C, E, H)** Paw withdrawal thresholds in response to static mechanical stimulation (von Frey assay) were measured on the ipsilateral paw at baseline and one day after paw incision. **(B)** Subcutaneous (SC) administration of TAFA4 significantly increased the threshold 2 hours post-injection in control mice but had no effect in *Nav1.8-LRP1* mice. **(C)** Intrathecal (IT) injection of TAFA4 significantly increased the threshold in both control and *Nav1.8-LRP1* mice. **(E)** SC injection of TAFA4 significantly increased mechanical thresholds in both *GINIP-DTR* and control mice. **(H)** Similar effects were observed in RTX-treated and control mice 2 hours after TAFA4 injection. **(F, I)** Diagrams representing the neuronal subpopulations ablated following: **(F)** Diphtheria toxin injection in *GINIP-DTR* mice, and **(I)** Resiniferatoxin (RTX) treatment.

All data are presented as mean ± SEM. Statistical analyses were conducted using two-way repeated measures ANOVA followed by Bonferroni post hoc tests. The number of mice per condition is indicated in parentheses.

Figure 3. Differential labeling of sensory neuron subtypes in Nav1.8-tdTomato and Advillin-tdTomato mice.

Representative images of lumbar DRG sections from *Nav1.8-tdTomato* and *Advillin-tdTomato* reporter mice double-immunostained for **(A)** NF200 (green) and tdTomato (red), **(B)** CGRP (green) and tdTomato (red), **(C)** TrkC (green) and tdTomato (red), **(D)** Parvalbumin (green) and tdTomato (red), **(E)** P2X3 (green) and tdTomato (red), **(F)** Tyrosine Hydroxylase (green) and tdTomato (red), (**G**) Quantification of the percentage of RFP positive neurons expressing each of the molecular markers. Statistical significance was determined using the Mann-Whitney test.

Figure 4. TAFA4/LRP1 signaling enhances phosphatase activity in Aβ-LTMRs.

(A) Volcano plot showing the mean log2 fold change (log2 HA-TAFA4/HA) of detected proteins and the corresponding -log10 of p-values when comparing protein intensities between HA-TAFA4 and HA conditions. Out of 1799 quantified proteins, 280 were significantly enriched in the HA-TAFA4 condition. Notably, LRP1 (red), TAFA4 (blue), and 23 phosphatases (green) were identified as enriched. **(B)** Gene ontology analysis indicating a significant enrichment of proteins involved in phosphatase activity. **(C)** Schematic of the phosphatase activity assay. Mouse sensory neurons are cultured for 24 hours, followed by 45-minute stimulation with or without TAFA4 (50 nM). Cell lysates are then incubated with DiFMUP to measure fluorescence. **(D)** Fluorescence-time curve showing phosphatase activity in cultured sensory neurons treated or not with TAFA4 (50 nM) and incubated with DiFMUP for 30 minutes. The slope indicates phosphatase activity. **(E-G)** Phosphatase activity normalized to vehicle treatment in sensory neurons cultured from various mouse strains. **(E)** TAFA4 increases phosphatase activity in C57BL6J mice. **(F)** TAFA4-mediated increase of phosphatase activity is abolished in Advillin-LRP1 and Nav1.8-LRP1 mice. **(G)** TAFA4 increases phosphatase activity in Plp1-LRP1, GINIP DTR, and RTX mice.

For normalization experiments, each dot represents an individual mouse. Results are shown as mean ± SEM. Statistical significance was determined using the Mann-Whitney test.

Figure 5. TAFA4 decreases mTORC1 phosphorylation through activation of AMPK

(A) Immunostaining for βIII-tubulin, mTORC1, and phospho-mTORC1 in DRG cultures from control and *Advillin-LRP1* mice, treated with vehicle or TAFA4 (50 nM) for 45 minutes. mTORC1 expression is restricted to neurons. TAFA4 increases phospho-mTORC1 levels in control but not in Advillin-LRP1 neurons. **(B)** Quantification of phospho-mTORC1 immunoreactivity in DRG cultures from control mice treated with vehicle or TAFA4 across four independent experiments. **(C)** Quantification of total mTOR protein levels in control DRG

cultures treated with vehicle or TAFA4 across three independent experiments. **(D, E)** Quantification of phospho-mTOR **(D)** and total mTOR **(E)** protein levels in DRG cultures from *Advillin-LRP1* mice treated with vehicle or TAFA4 across three independent experiments. The numbers displayed in each bar in Figures B to E indicate the total number of cells used for quantification in each condition.

TAFA4 treatment does not affect phospho-mTOR levels in *Advillin-LRP1* cultures. **(F)** Western blot analysis of p70S6K phosphorylation at Thr/Ser residues and total p70S6K protein, 45 minutes post-treatment with vehicle or TAFA4 and Quantification of p70S6K phosphorylation normalized to total p70S6K protein levels. **(G)** Western blot analysis of ERK, Akt, and AMPK phosphorylation following 45-minute incubation with vehicle or TAFA4. **(H)** Quantification of phosphorylated ERK, Akt, and AMPK levels normalized to α-tubulin. TAFA4 selectively and significantly increases AMPK phosphorylation compared to ERK and Akt. The data represented in panels **F and G** were performed four times using DRG cultures from 10 mice and those in figure H were performed three times. (I) Intraplantar injection of compound C significantly reduces TAFA4-induced analgesia in a paw incision pain model. The number of mice is indicated in the figure panel. **(J)** SC administration of TAFA4 failed to trigger pain relief in mice lacking TSC2 in DRG neurons. All data are presented as mean ± SEM. Statistical analyses were performed using unpaired t-tests and two-way repeated measures ANOVA followed by Bonferroni post hoc tests.

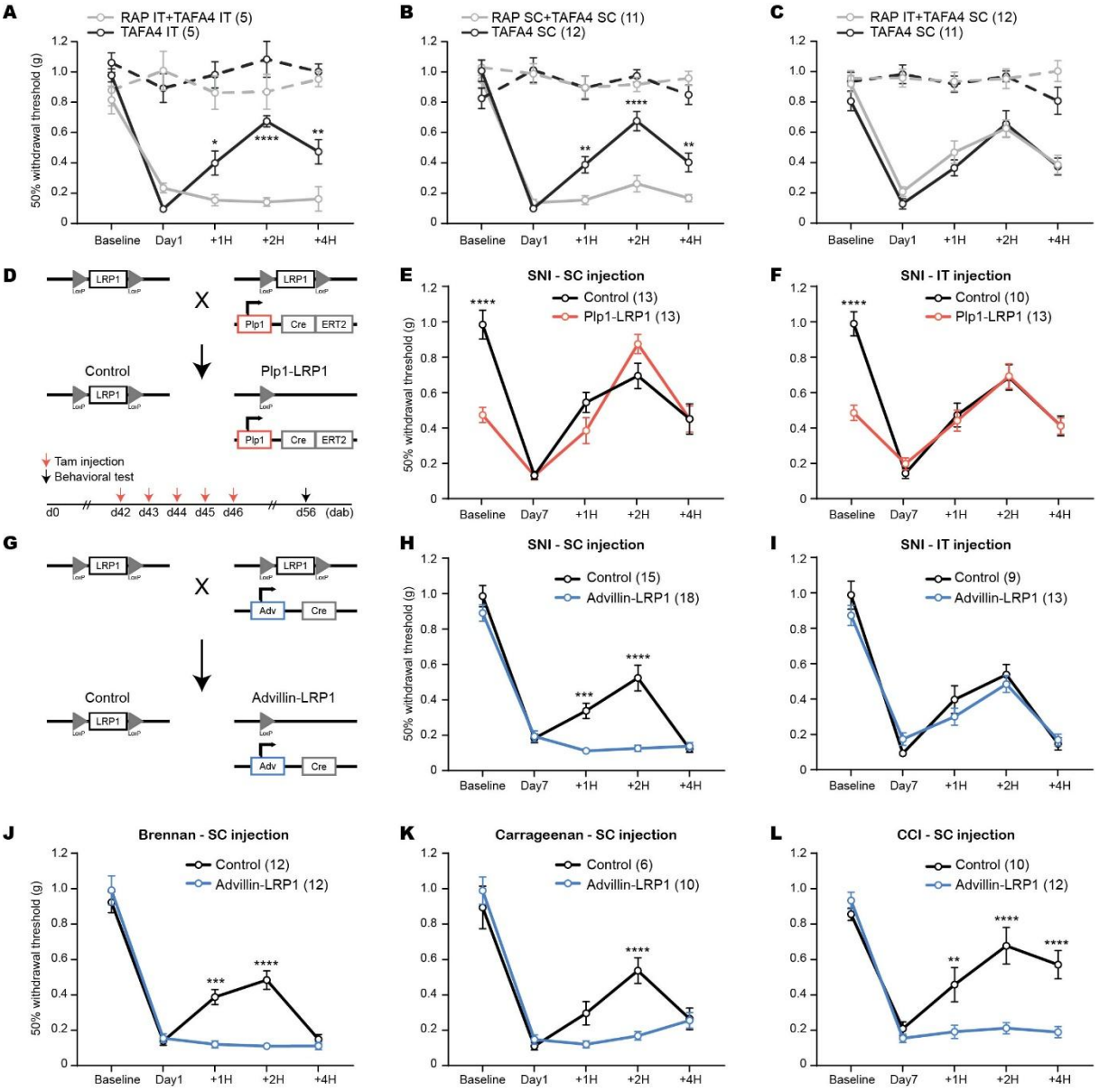
A
RAP IT+TAFA4 IT (5)
TAFA4 IT (5)
50% withdrawal threshold (g)
Baseline
Day1
+1H
+2H
+4H
B
RAP SC+TAFA4 SC (11)
TAFA4 SC (12)
C
RAP IT+TAFA4 SC (12)
TAFA4 SC (11)
D
LRP1
Plp1
Cre
ERT2
Control
Plp1-LRP1
Tam injection
Behavioral test
d0
d42
d43
d44
d45
d46
d56
(dab)
E
SNI - SC injection
Control (13)
Plp1-LRP1 (13)
Day7
F
SNI - IT injection
Control (10)
Plp1-LRP1 (13)
G
Adv
Advillin-LRP1
H
SNI - SC injection
Control (15)
Advillin-LRP1 (18)
I
SNI - IT injection
Control (9)
Advillin-LRP1 (13)
J
Brennan - SC injection
Control (12)
Advillin-LRP1 (12)
K
Carrageenan - SC injection
Control (6)
Advillin-LRP1 (10)
L
CCI - SC injection
Control (10)
Advillin-LRP1 (12)

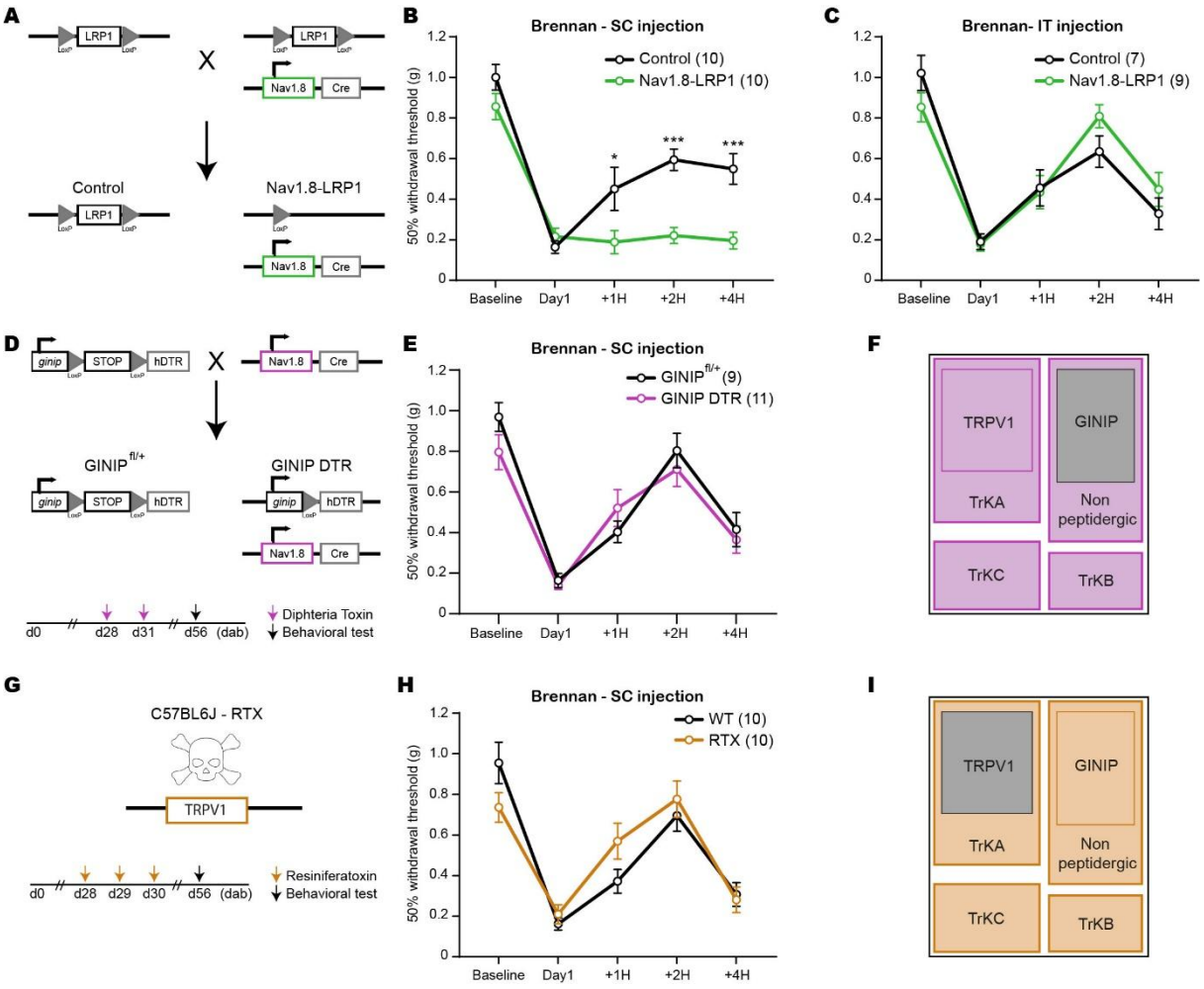
A
LRP1
LoxP
X
Nav1.8
Cre
Control
Nav1.8-LRP1
B
Brennan - SC injection
Control (10)
Nav1.8-LRP1 (10)
50% withdrawal threshold (g)
Baseline
Day1
+1H
+2H
+4H
C
Brennan- IT injection
Control (7)
Nav1.8-LRP1 (9)
D
ginip
STOP
hDTR
GINIP fl/+
GINIP DTR
d0
d28
d31
d56 (dab)
Diphteria Toxin
Behavioral test
E
Brennan - SC injection
GINIP fl/+ (9)
GINIP DTR (11)
F
TRPV1
GINIP
TrKA
Non peptidergic
TrKC
TrKB
G
C57BL6J - RTX
TRPV1
d0
d28
d29
d30
d56 (dab)
Resiniferatoxin
Behavioral test
H
Brennan - SC injection
WT (10)
RTX (10)
I
TRPV1
GINIP
TrKA
Non peptidergic
TrKC
TrKB

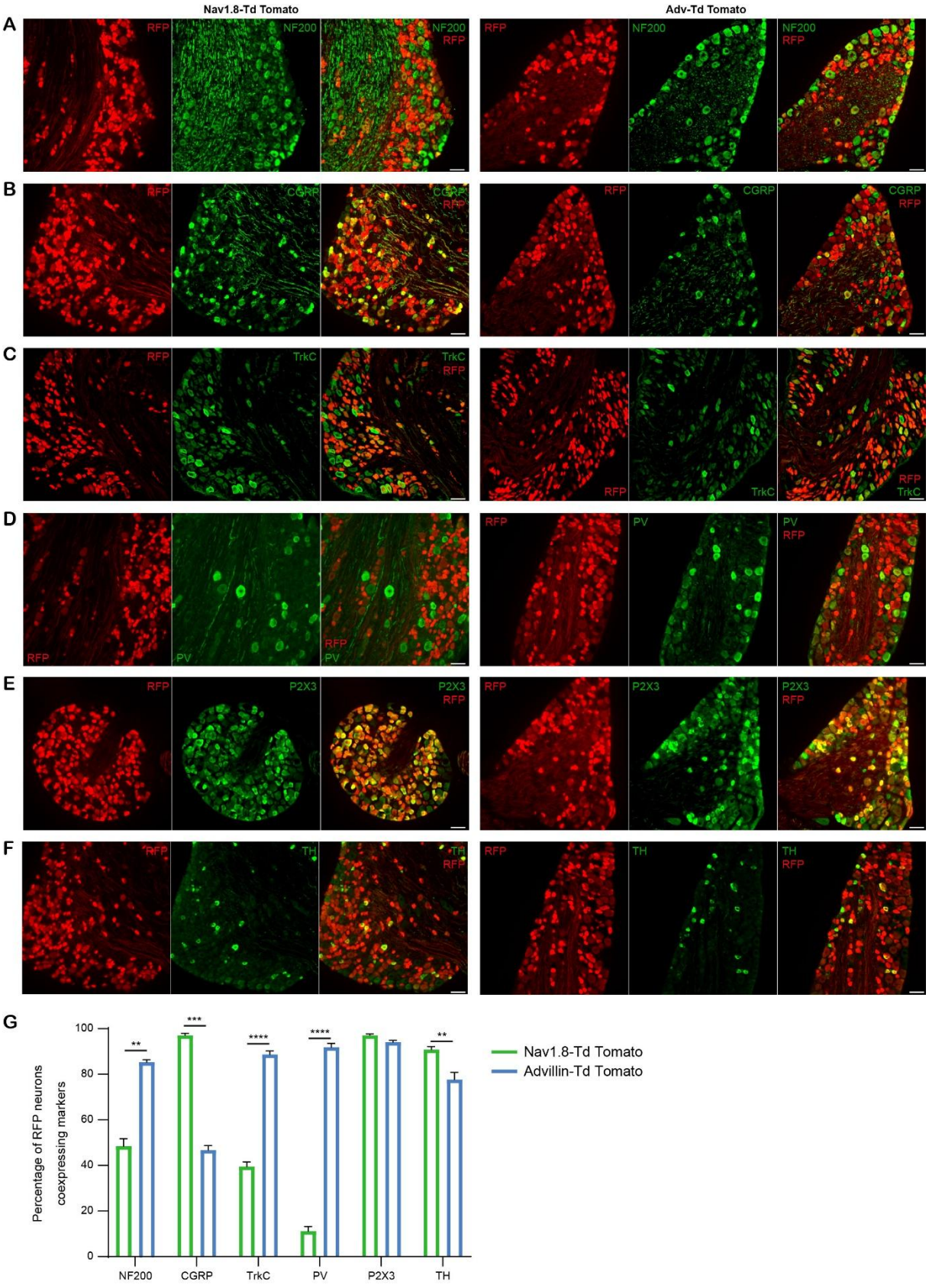
Nav1.8-Td Tomato
Adv-Td Tomato
A
RFP
NF200
NF200
RFP
B
CGRP
C
TrkC
D
PV
E
P2X3
F
TH
G
Percentage of RFP neurons coexpressing markers
100
80
60
40
20
0
**
***
****
****
**
NF200
CGRP
TrkC
PV
P2X3
TH
Nav1.8-Td Tomato
Advillin-Td Tomato

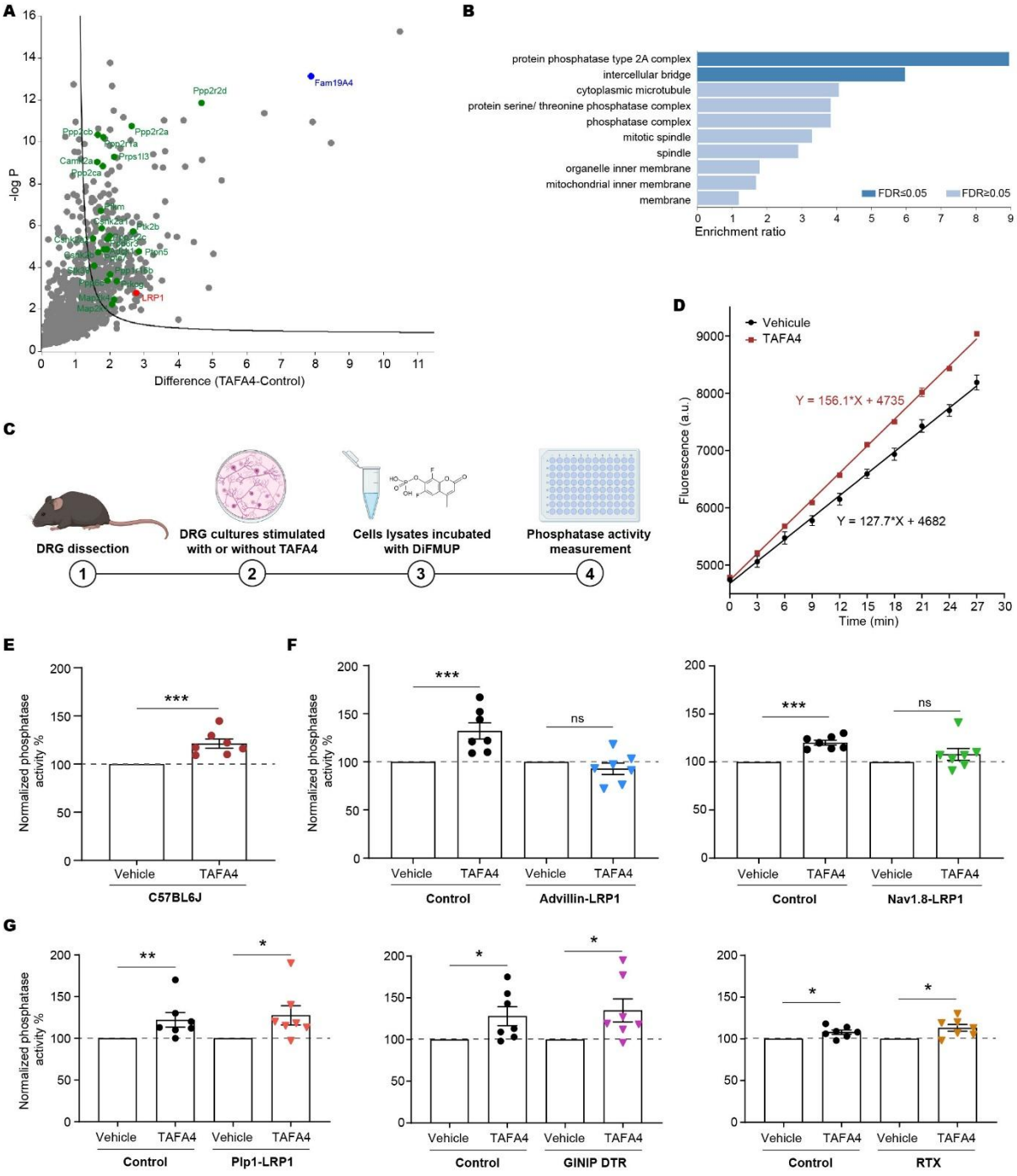
A
-log P
Difference (TAFA4-Control)
Fam19A4
Ppp2r2d
Ppp2r2a
Ppp2cb
Ppp2ca
Prps1l3
Ptk2b
Ptpn5
LRP1
B
protein phosphatase type 2A complex
intercellular bridge
cytoplasmic microtubule
protein serine/ threonine phosphatase complex
phosphatase complex
mitotic spindle
spindle
organelle inner membrane
mitochondrial inner membrane
membrane
FDR≤0.05
FDR≥0.05
Enrichment ratio
C
DRG dissection
DRG cultures stimulated with or without TAFA4
Cells lysates incubated with DiFMUP
Phosphatase activity measurement
1
2
3
4
D
Vehicule
TAFA4
Y = 156.1*X + 4735
Y = 127.7*X + 4682
Fluorescence (a.u.)
Time (min)
E
Normalized phosphatase activity %
***
Vehicle
TAFA4
C57BL6J
F
***
ns
Control
Advillin-LRP1
Nav1.8-LRP1
G
**
*
Plp1-LRP1
GINIP DTR
RTX

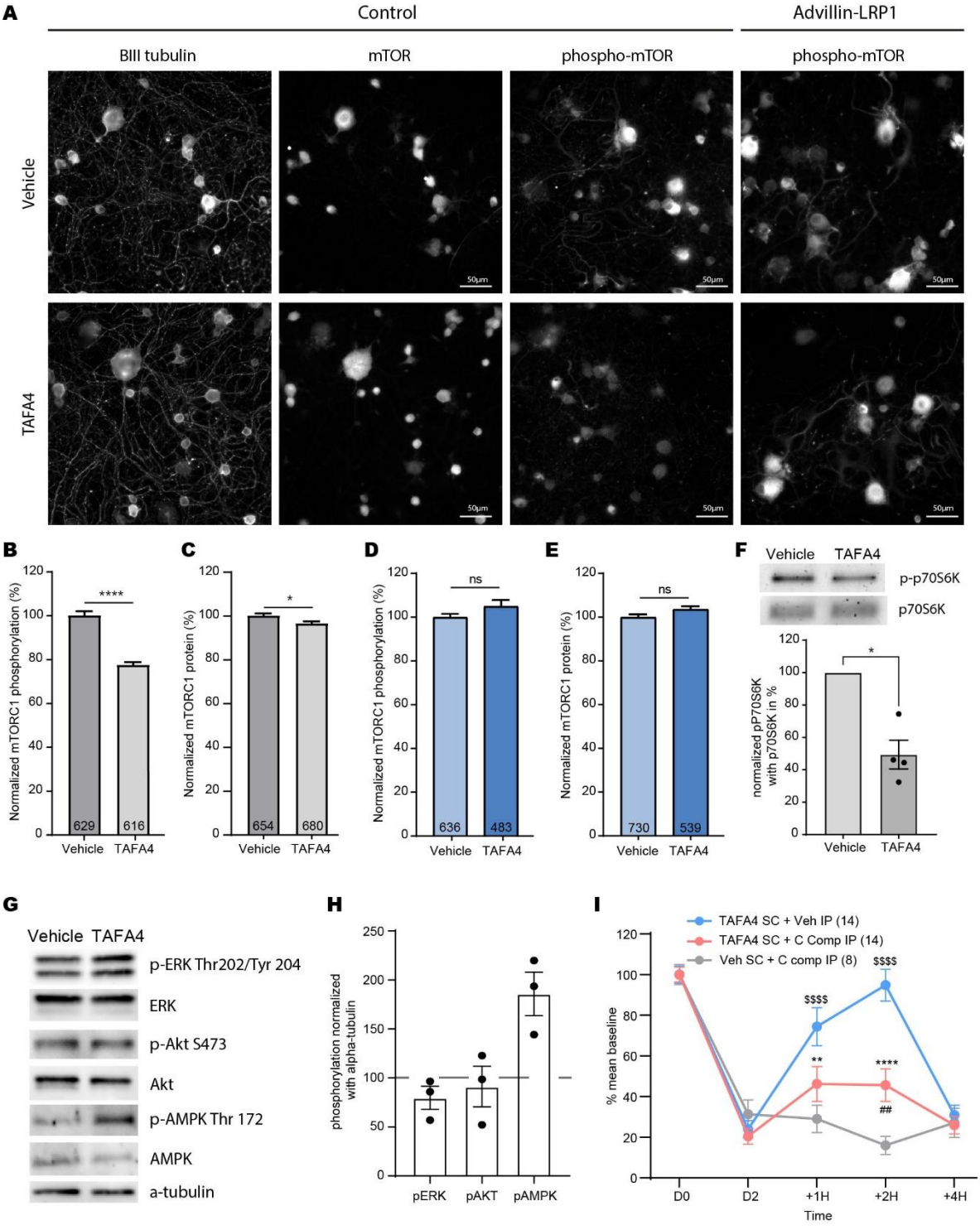
A
Control
Advillin-LRP1
BIII tubulin
mTOR
phospho-mTOR
phospho-mTOR
Vehicle
TAFA4
50µm
B
Normalized mTORC1 phosphorylation (%)
****
629
616
Vehicle
TAFA4
C
Normalized mTORC1 protein (%)
*
654
680
Vehicle
TAFA4
D
Normalized mTORC1 phosphorylation (%)
ns
636
483
Vehicle
TAFA4
E
Normalized mTORC1 protein (%)
ns
730
539
Vehicle
TAFA4
F
Vehicle
TAFA4
p-p70S6K
p70S6K
normalized pP70S6K with p70S6K in %
*
Vehicle
TAFA4
G
Vehicle
TAFA4
p-ERK Thr202/Tyr 204
ERK
p-Akt S473
Akt
p-AMPK Thr 172
AMPK
a-tubulin
H
phosphorylation normalized with alpha-tubulin
pERK
pAKT
pAMPK
I
TAFA4 SC + Veh IP (14)
TAFA4 SC + C Comp IP (14)
Veh SC + C comp IP (8)
$$$$
$$$$
**
****
##
% mean baseline
D0
D2
+1H
+2H
+4H
Time
J
Control (15)
Advillin-Tsc2 (21)
*
**
% mean baseline
D0
D1
+1H
+2H
+4H
Time

Supplementary Files

This is a list of supplementary files associated with this preprint. Click to download.

- CharronetalSupportingInformation.pdf
- Rawdatafigures5Fand5G.pdf